Laboratoire d'Annecy-le-Vieux de Physique des Particules

Measurement of the transverse momentum distribution of Drell-Yan electron pairs using the ϕ^*_η variable with the ATLAS detector

Presented by: **Thi Kieu Oanh DOAN**

To obtain: **Doctoral degree**

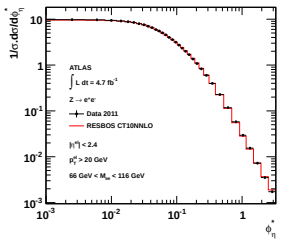

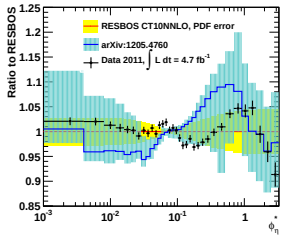

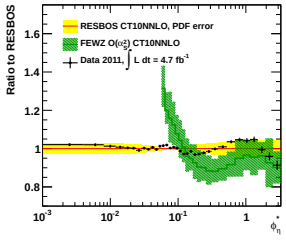

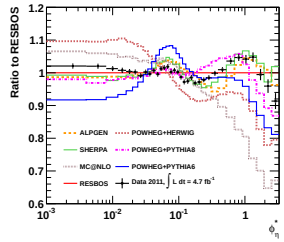

Contents

Theoretical review

Standard Model

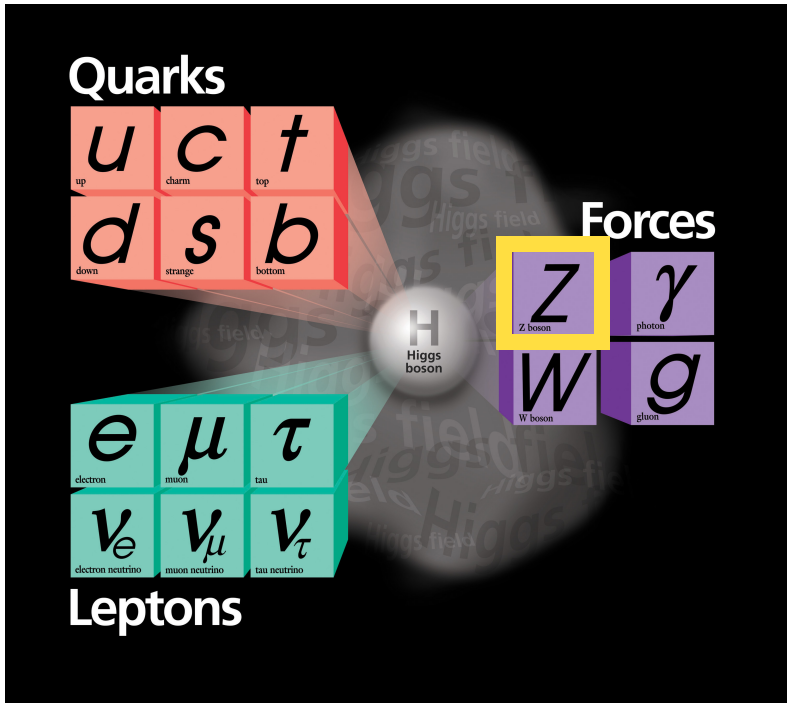

Z boson

- Postulated in the Glashow-Weinberg-Salam model in the 1960s and first discovered at SP$\bar{\text{P}}$S in 1983.
- Properties (mass and width) were precisely measured at LEP.
- Important probe for physics at hadron colliders.

Z production and decay at hadron colliders

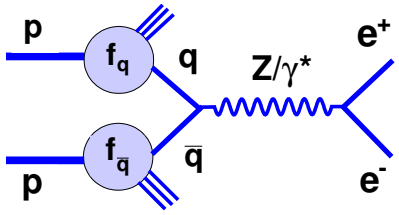

- Well known cross section
- Calculated up to NNLO

Phys. Rev., D85:072004, 2012.

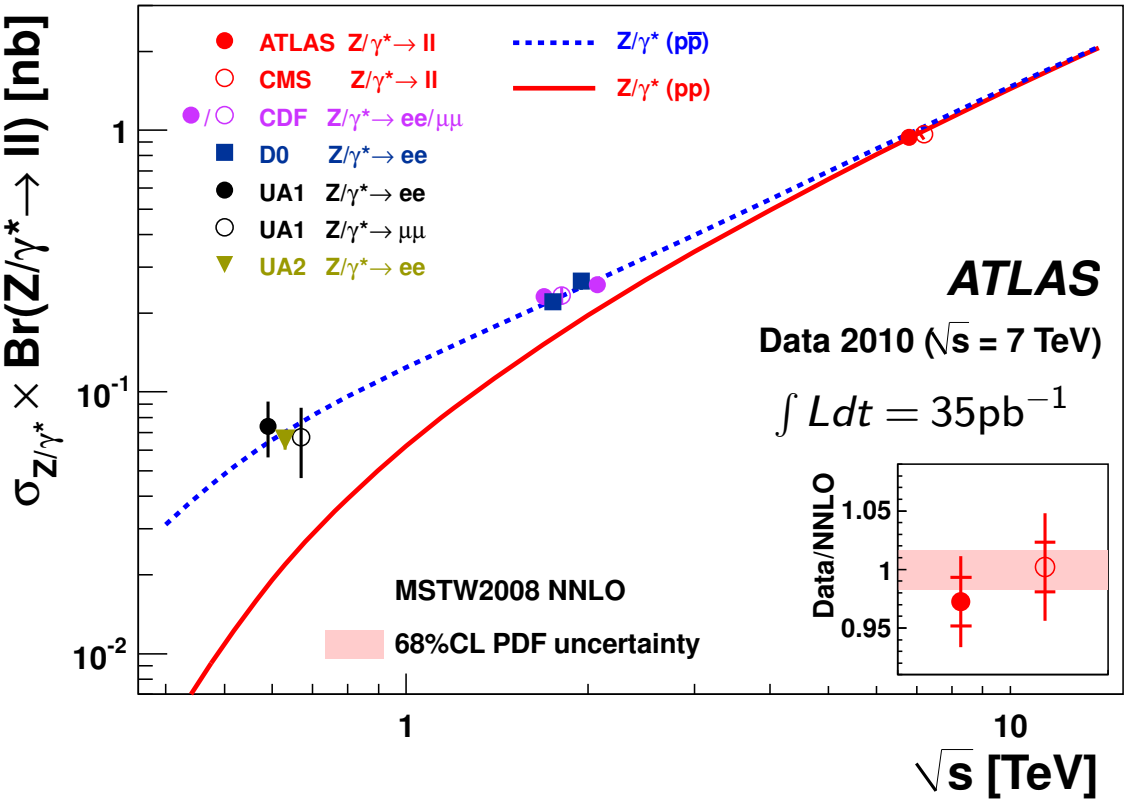

High statistic data sample in 2011: $\int Ldt = 4.7\text{fb}^{-1}$

$\to$ physics studies with the high precision.

p_T^Z predictions at hadron colliders

- At LO: $p_T^Z = 0$
- Beyond LO: $\frac{d\sigma}{dp_T^2}$ can be expressed in powers of α_s

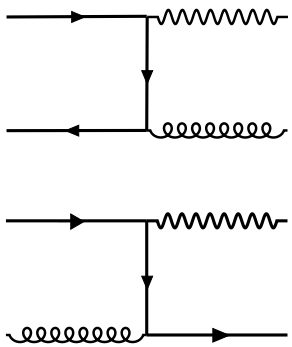

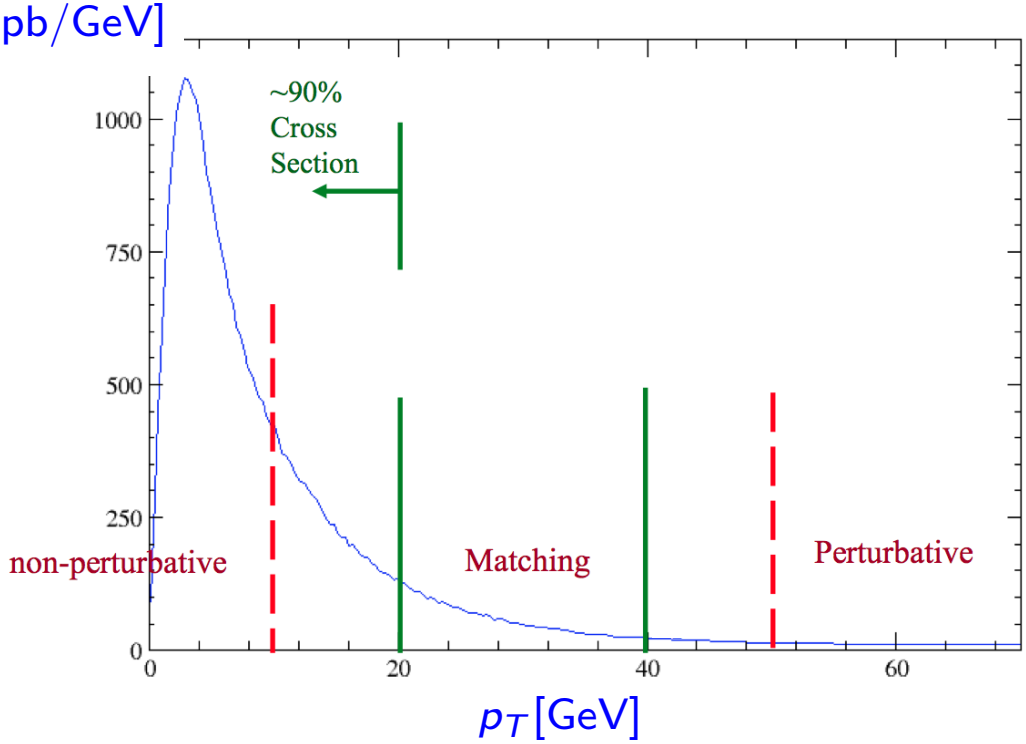

For high $p_T^Z \to$ the contribution of higher orders in α_s decreases quickly $\to$ a perturbative calculation is applicable.

- At NLO ($\mathcal{O}(\alpha_s)$), ($Q^2 = M_Z^2$):

$$\frac{d\sigma}{dp_T^2} = \alpha_s \left(A \frac{\ln(Q^2/p_T^2)}{p_T^2} + B \frac{1}{p_T^2} + C(p_T^2) \right),$$

where A and B are calculable coefficients and C is an integrable function.

p_T^Z predictions at hadron colliders at low p_T^Z

(Soft and collinear gluon emissions)

Dominant contributions to the differential cross section ($Q^2 = M_Z^2$):

$$\frac{d\sigma}{dp_T^2} \sim \frac{\alpha_s}{p_T^2} \ln\left(\frac{Q^2}{p_T^2}\right)\left[v_1 + v_2\alpha_s \ln^2\left(\frac{Q^2}{p_T^2}\right) + v_3\alpha_s^2 \ln^4\left(\frac{Q^2}{p_T^2}\right) + ...\right]$$

For $p_T \to 0$, $\alpha_s \ln^2(Q^2/p_T^2)$ is large even when α_s is small

$\to$ the p_T distribution diverges.

$\to$ Two approaches:

- Applying resummation of leading logarithms to all orders in α_s.

(RESBOS: Resummation + NLO corrected to $\mathcal{O}(\alpha_s^2)$ using $K-$factor)

- Or modeling by parton shower generators.

Motivations of the p_T^Z measurement

1. Provide an ideal testing of pQCD.
2. Study the low p_T^Z region where non-perturbative effects may play a role.
3. Improve the modelling of W boson production needed for a precise measurement of the W mass.
4. Important implications for understanding Higgs production.

Optimization of new variables to study p_T^Z

Why new variables?

The measurement at low p_T^Z is limited by the experimental resolution rather than the event statistics in particular for the electron channel.

Phys. Rev. D 86, 052010 (2012)

Main systematic uncertainties of the latest p_T^Z measurement:

Calorimeter response modeling $\oplus$ Unfolding $\sim 1\%$.

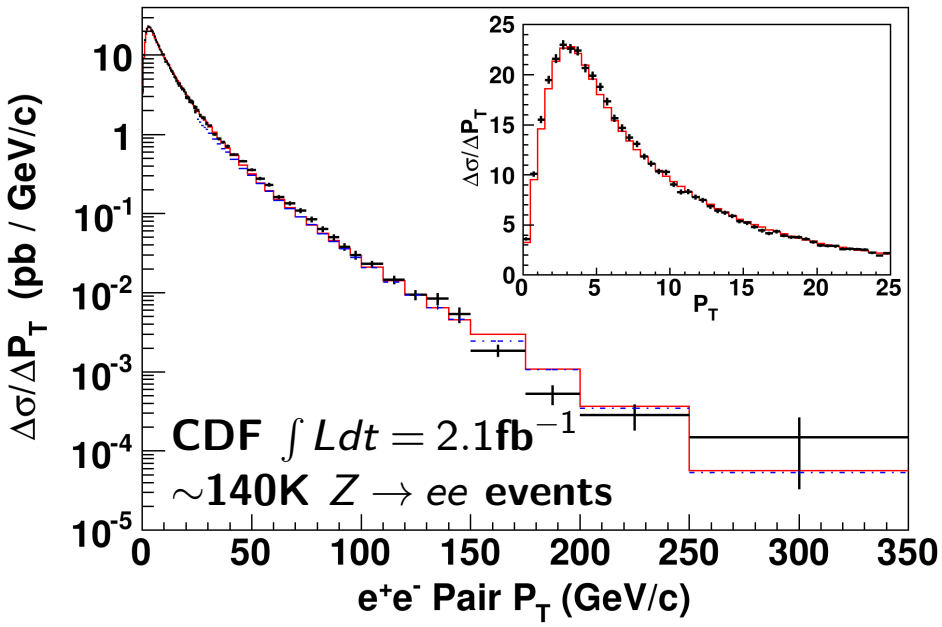

$\Longrightarrow$ Optimize new variables:

- less sensitive to the effects of experimental resolution.

- probe the same physical effects as p_T^Z.

New variables to study p_T^Z

Phys J. C, 71:1600, 2011.

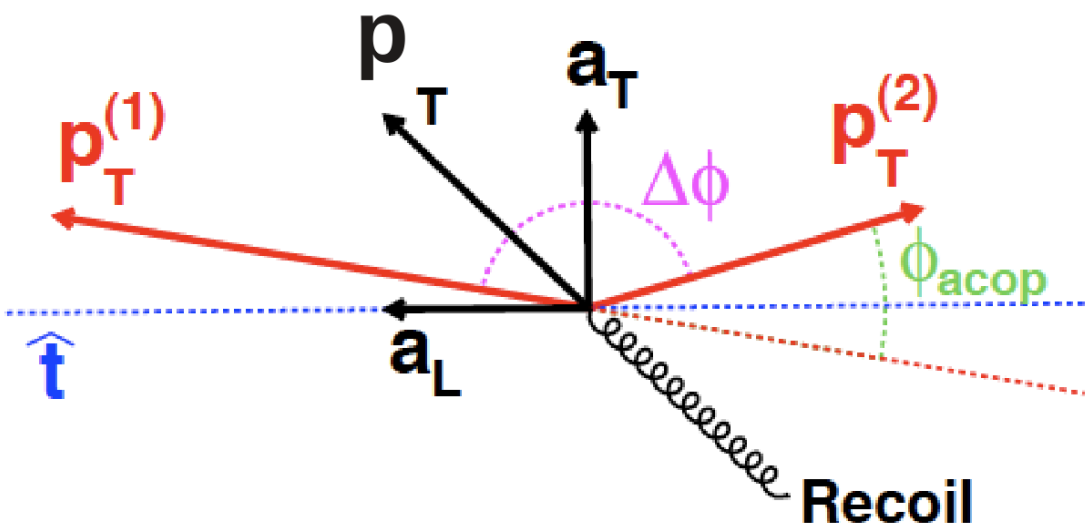

$$\hat{t} = (p_T^{(1)} - p_T^{(2)}) / |p_T^{(1)} - p_T^{(2)}|$$

$$p_T \rightarrow a_T \rightarrow a_T/m_Z \overset{p_T^{(1)} \approx p_T^{(2)}}{\approx} \tan(\phi_{acop}/2)\sin(\theta^*)$$

where θ^* is the scattering angle of the leptons relative to the beam direction in the dilepton rest frame.

The ϕ_η^* variable

- θ^* is still sensitive to the effects of lepton momentum resolution.
- θ_η^* is an alternative way to estimate the scattering angle:

$\cos(\theta_\eta^*) = \tanh(\frac{\eta^- - \eta^+}{2})$

$$a_T/m_Z \overset{p_T^{(1)} \approx p_T^{(2)}}{\approx} \tan(\phi_{acop}/2)\sin(\theta^*) \quad \to \quad \phi_\eta^* \equiv \tan(\phi_{acop}/2)\sin(\theta_\eta^*)$$

ϕ_η^* is based entirely on the measured track directions.

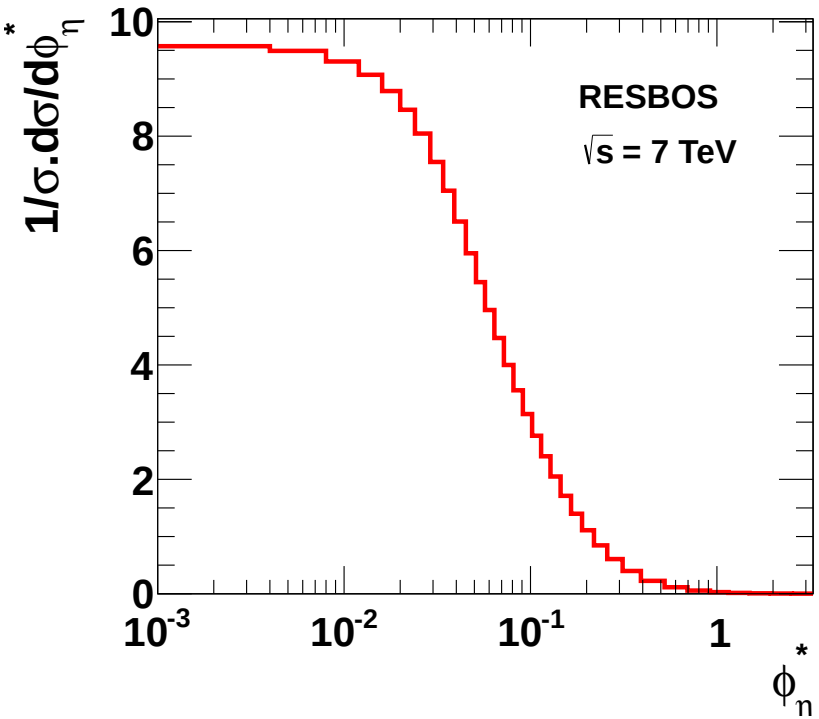

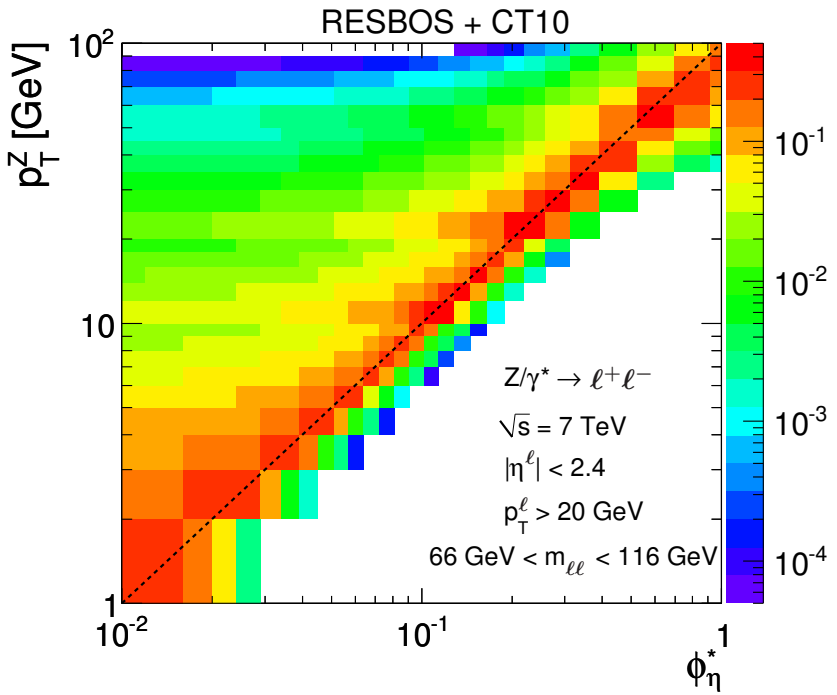

Comparison of new variables to study p_T^Z

Dependence on the ATLAS detector resolution effect

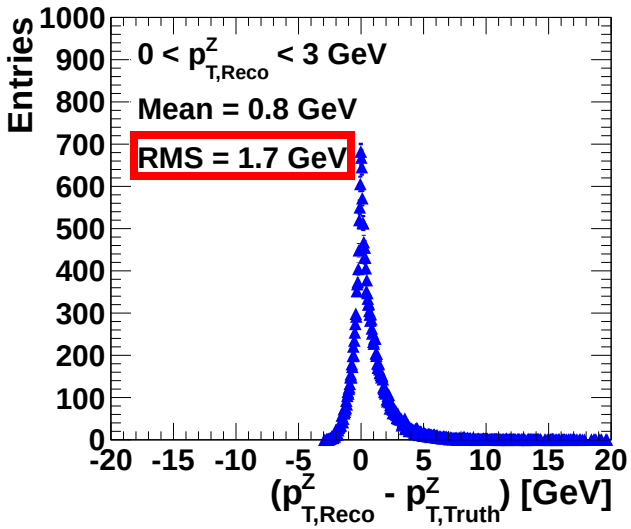

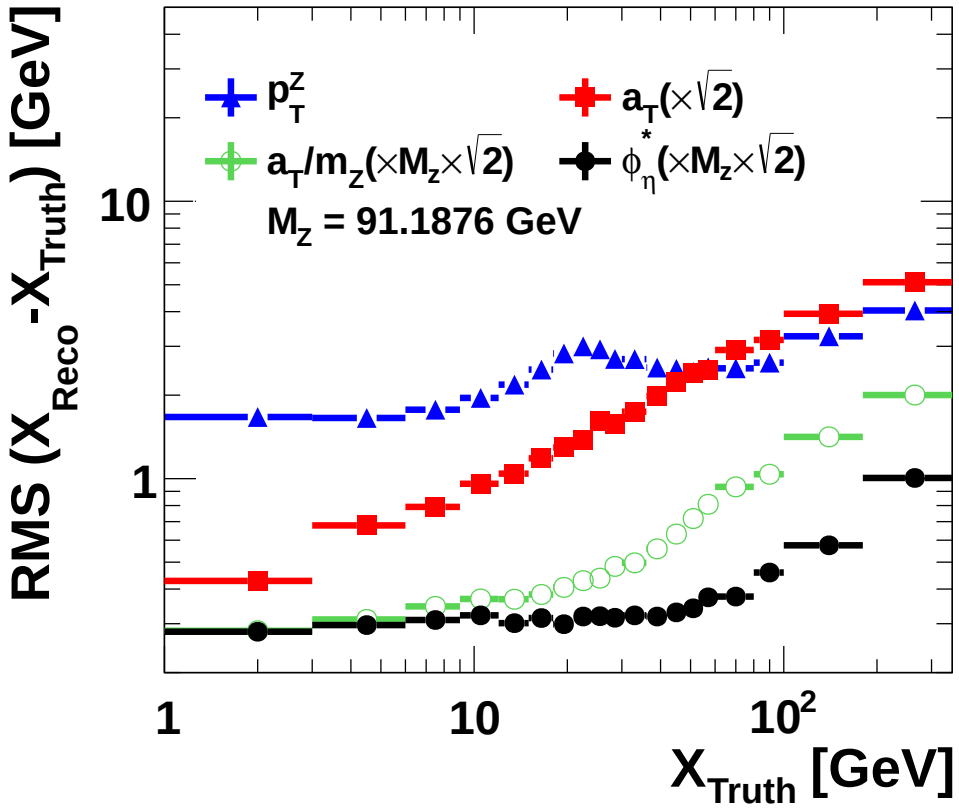

This method was proposed and used in Phys J. C, 71:1600, 2011.

$\to \phi^*_\eta$ has the best resolution in comparison with other variables to study p_T^Z.

The first measurement of the ϕ^*_η spectrum by D0

Phys.Rev.Lett. 106 (2011) 122001

@ 1.96 TeV $p\bar{p}$ collisions:

$\int Ldt = 7.3\text{fb}^{-1}$, $\sim$ 1M $Z \to ee + Z \to \mu\mu$ events.

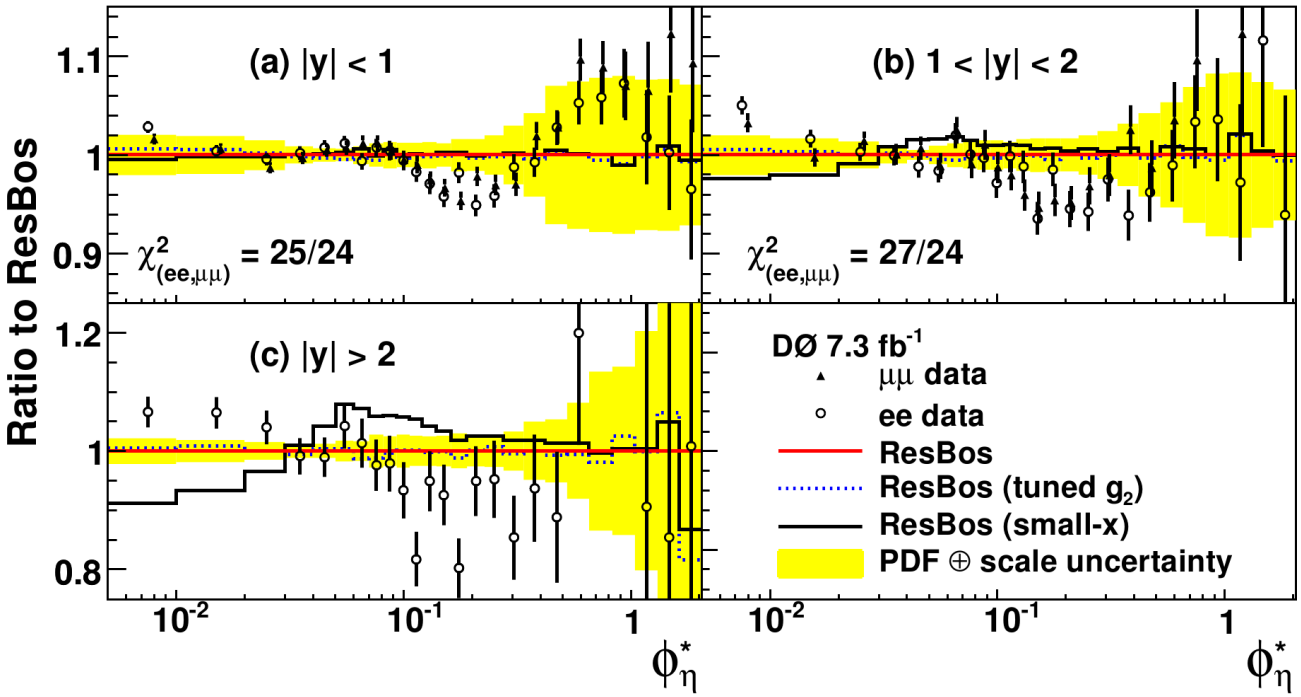

ATLAS 2011 data with $\int Ldt = 4.7\text{fb}^{-1}$, $\sim$ 3M $Z \to ee + Z \to \mu\mu$ events will be used for the first ϕ^*_η measurement @ $\sqrt{s} = 7$ TeV pp collisions @ LHC.

The LHC and the ATLAS detector

The LHC

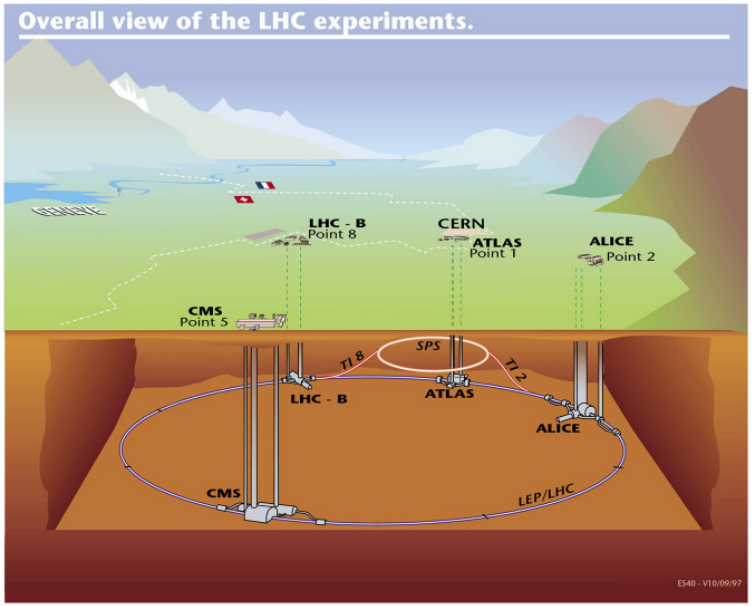

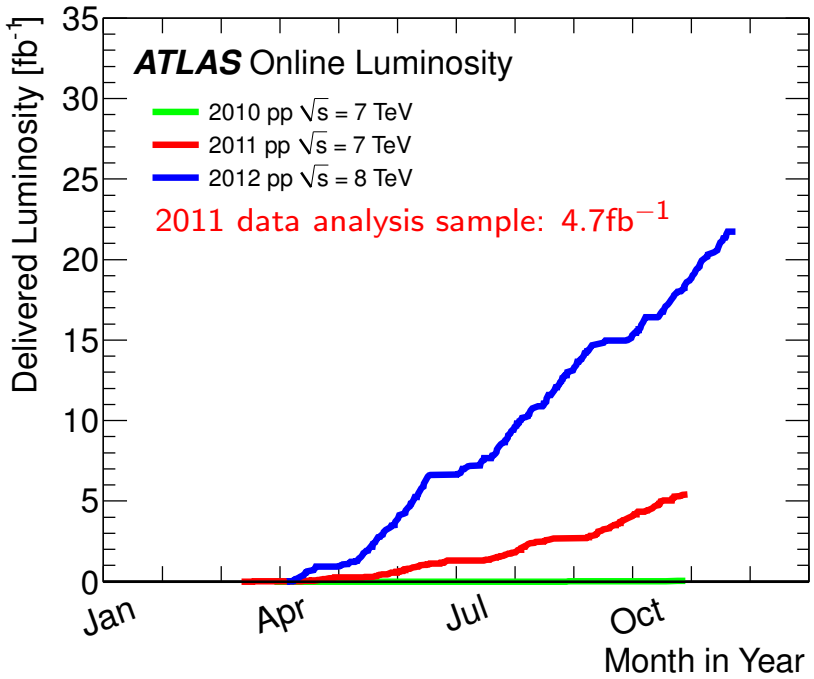

Beam parameter	Nominal	October 2011
Proton energy [TeV]	7	3.5
Bunch spacing [ns]	25	50
Peak luminosity $[cm^{-2}s^{-1}]$	10^{34}	3.6×10^{33}
Average peak pile-up	~ 20	18

"Pile-up": average number of interations in each bunch crossing.

The ATLAS detector

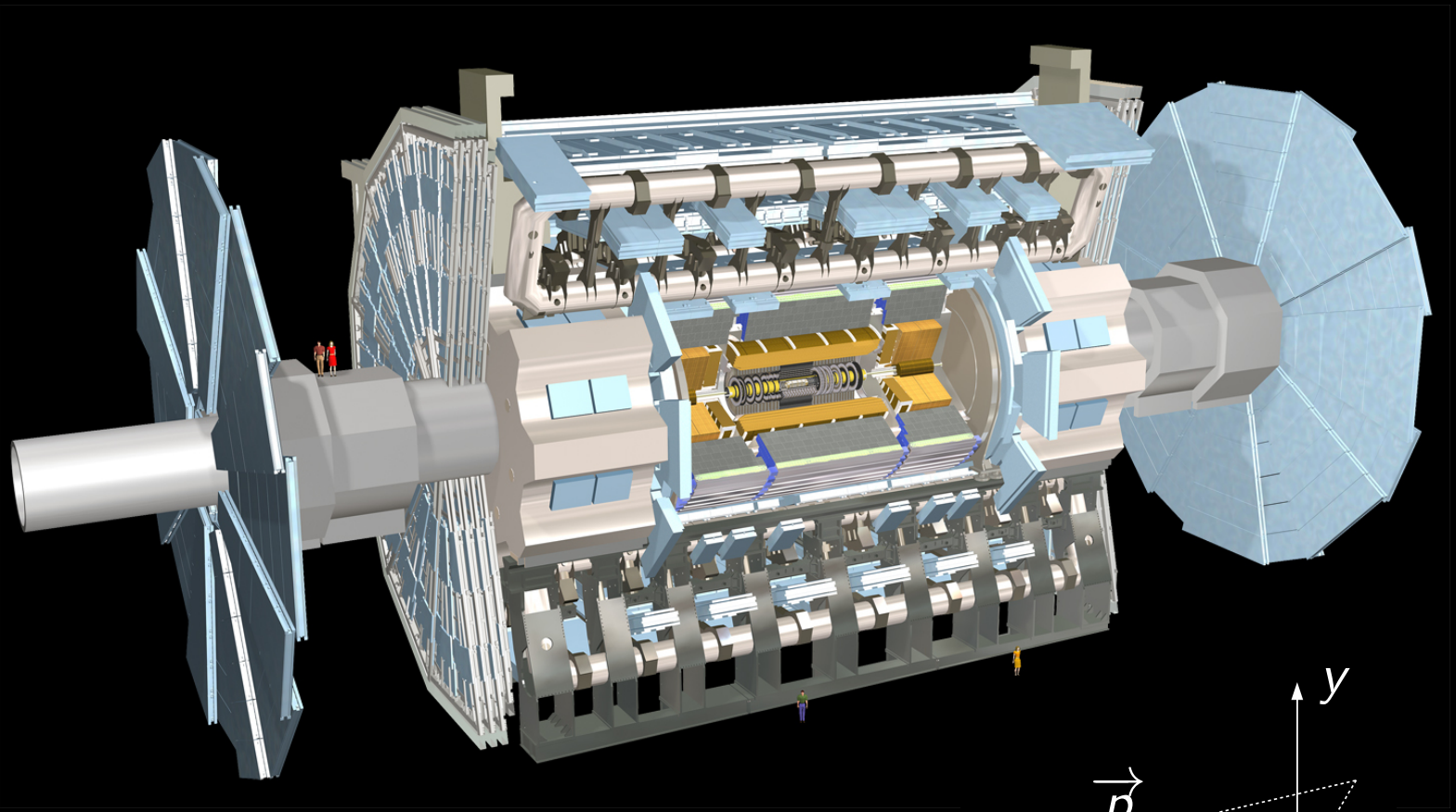

$$\eta = -\ln\left[\tan\left(\frac{\theta}{2}\right)\right]$$

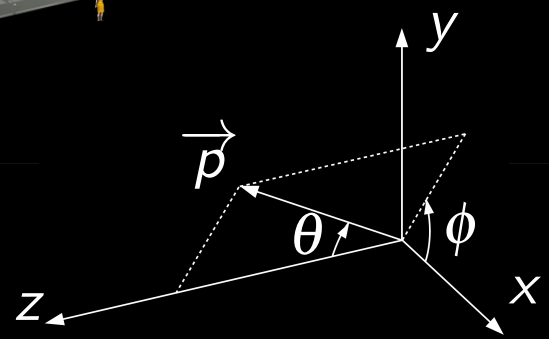

An electron is reconstructed as a track in the inner detector matched to a cluster in the calorimeters

The Inner Detector

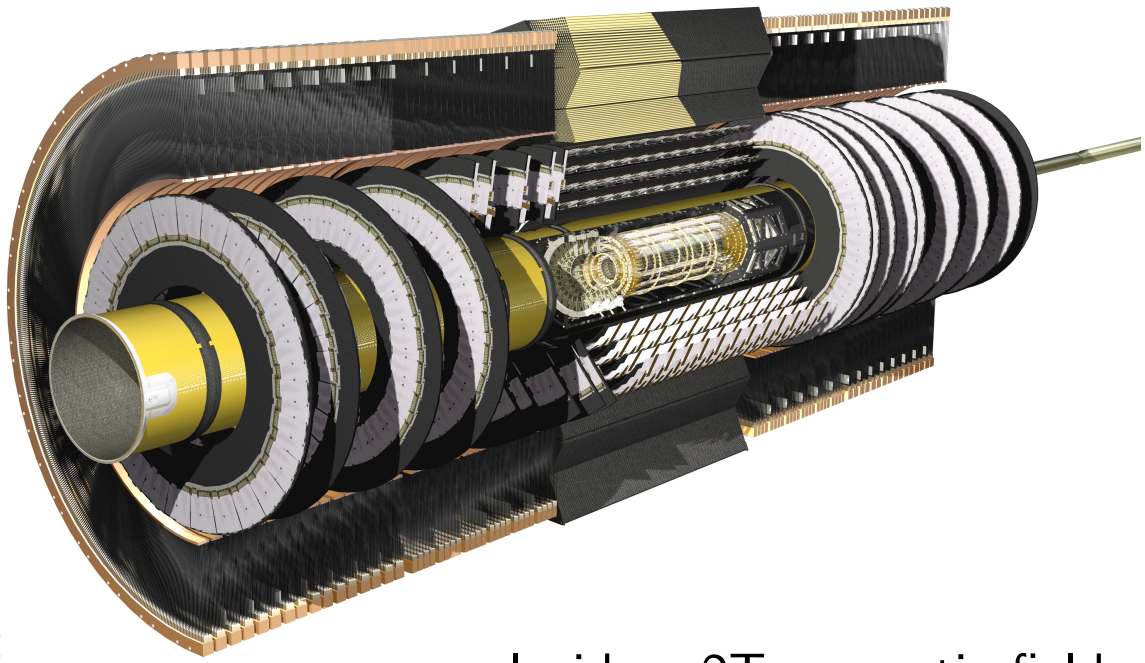

Consists of:

- Pixel detector
- Semiconductor tracker
- Transition radiation tracker

Inside a 2T magnetic field
$\to$ precise track measurements.

Resolution	$\lvert\eta\rvert$ coverage
$\sigma_{p_T}/p_T = 0.05\% p_T \oplus 1\%$ $\sigma_\phi = 0.6$ mrad $\sigma_\eta = 0.0012$	2.5

Track reconstruction

The ϕ^*_η measurement is based entirely on the measured track directions of electrons

$\to$ bremsstrahlung recovery algorithms are important to improve the precision of this measurement.

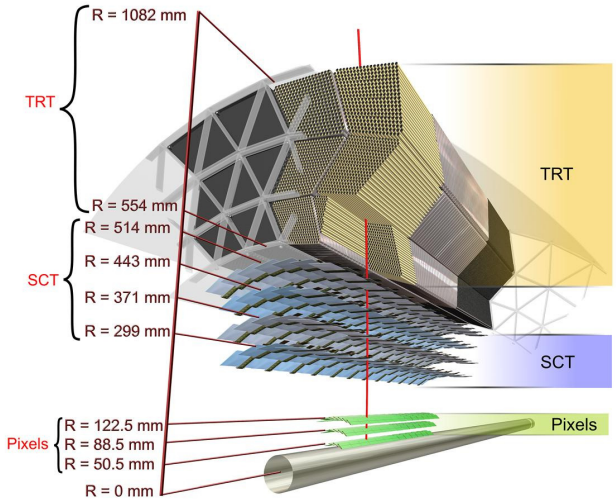

Gaussian-sum filter (GSF):

- Electron energy loss is approximated by a sum of Gaussians.
- Track parameters are represented by weighted sum of Gaussians.

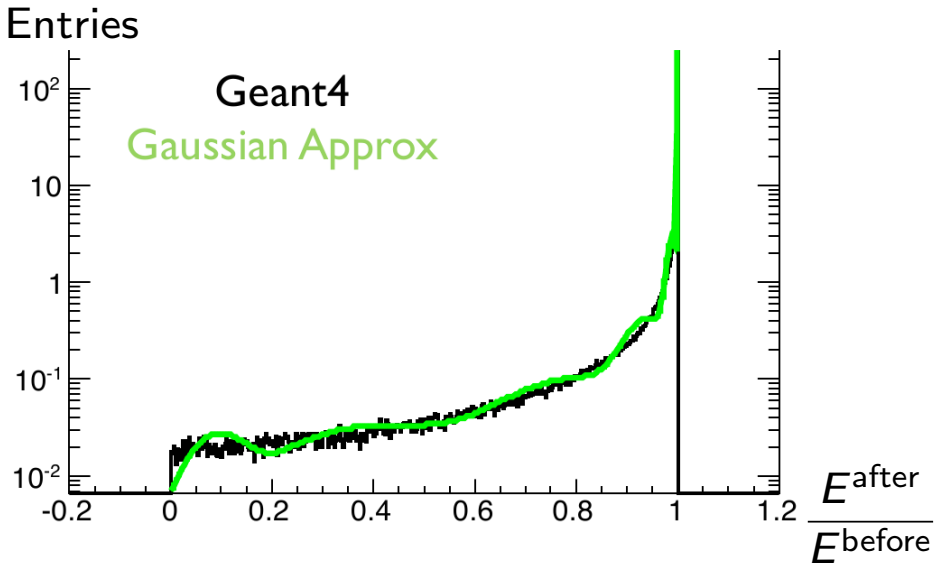

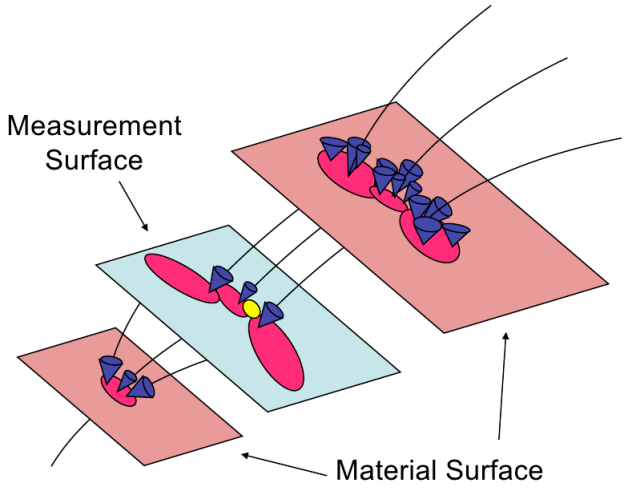

Track reconstruction in the Inner Detector

GSF electron track performance: resolution of track direction ϕ at the perigee

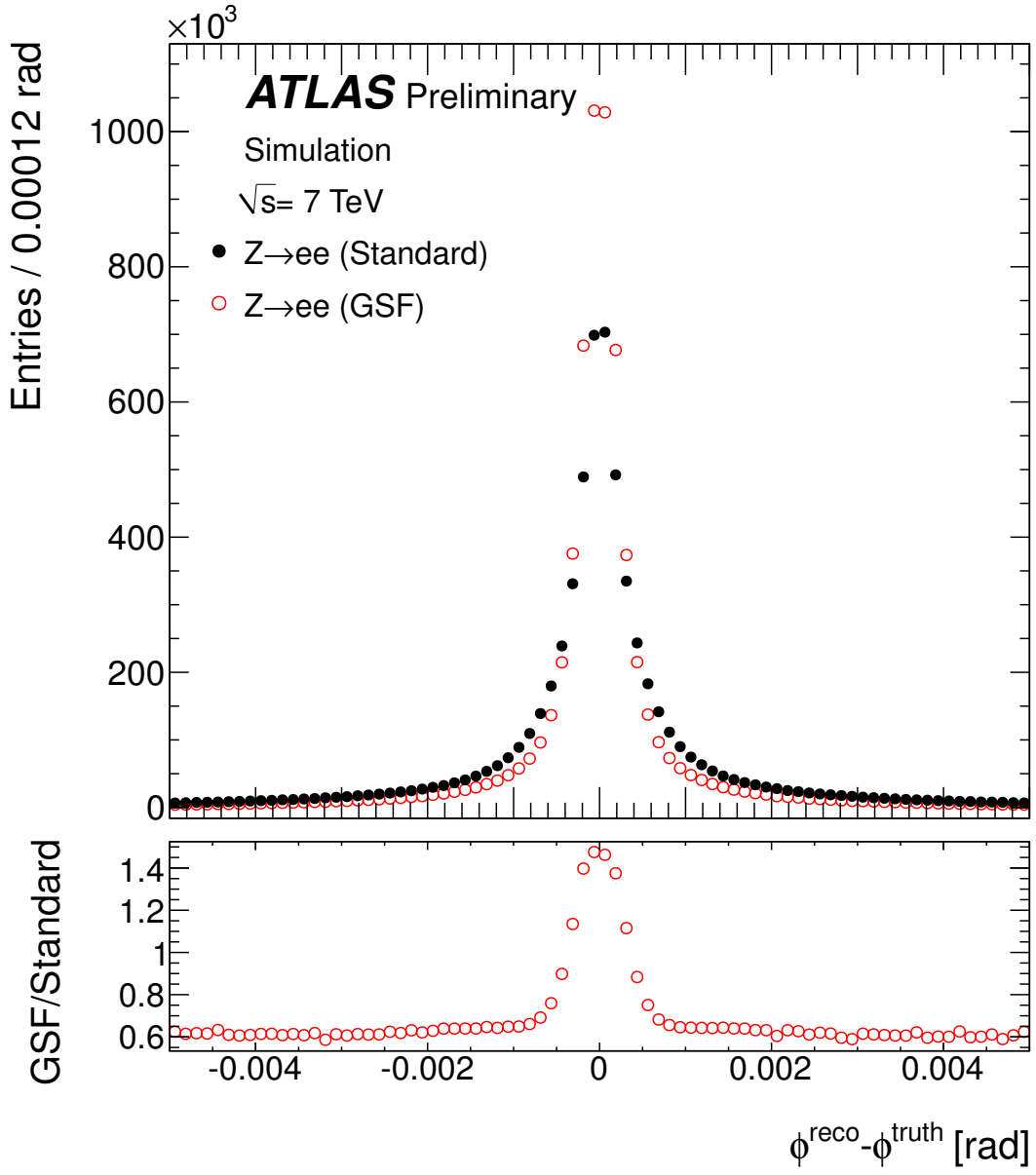

The electromagnetic calorimeters

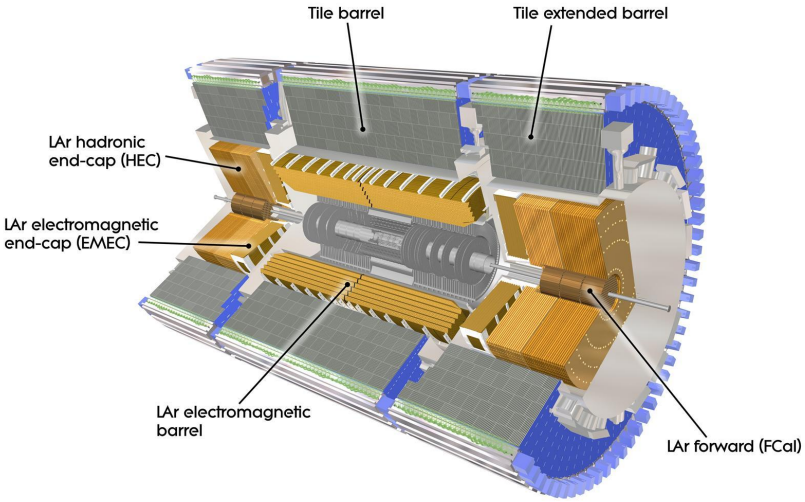

Electromagnetic Barrel

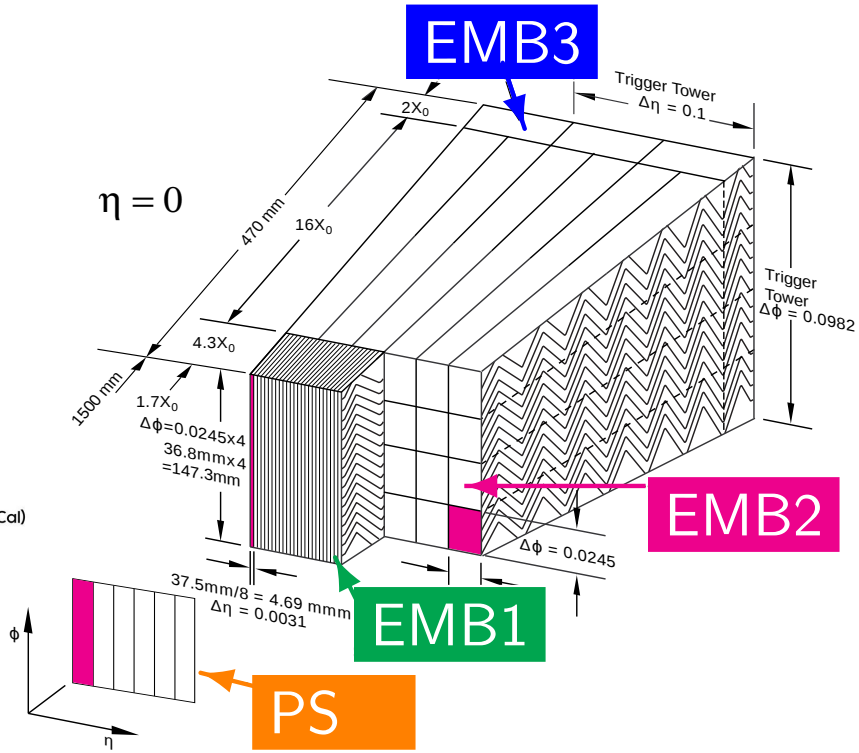

Detector component	Resolution	$\lvert\eta\rvert$ coverage
EM calorimeters	$\sigma_E/E = 10\%/\sqrt{E} \oplus 0.7\%$	3.2

Electron reconstruction: cluster energy

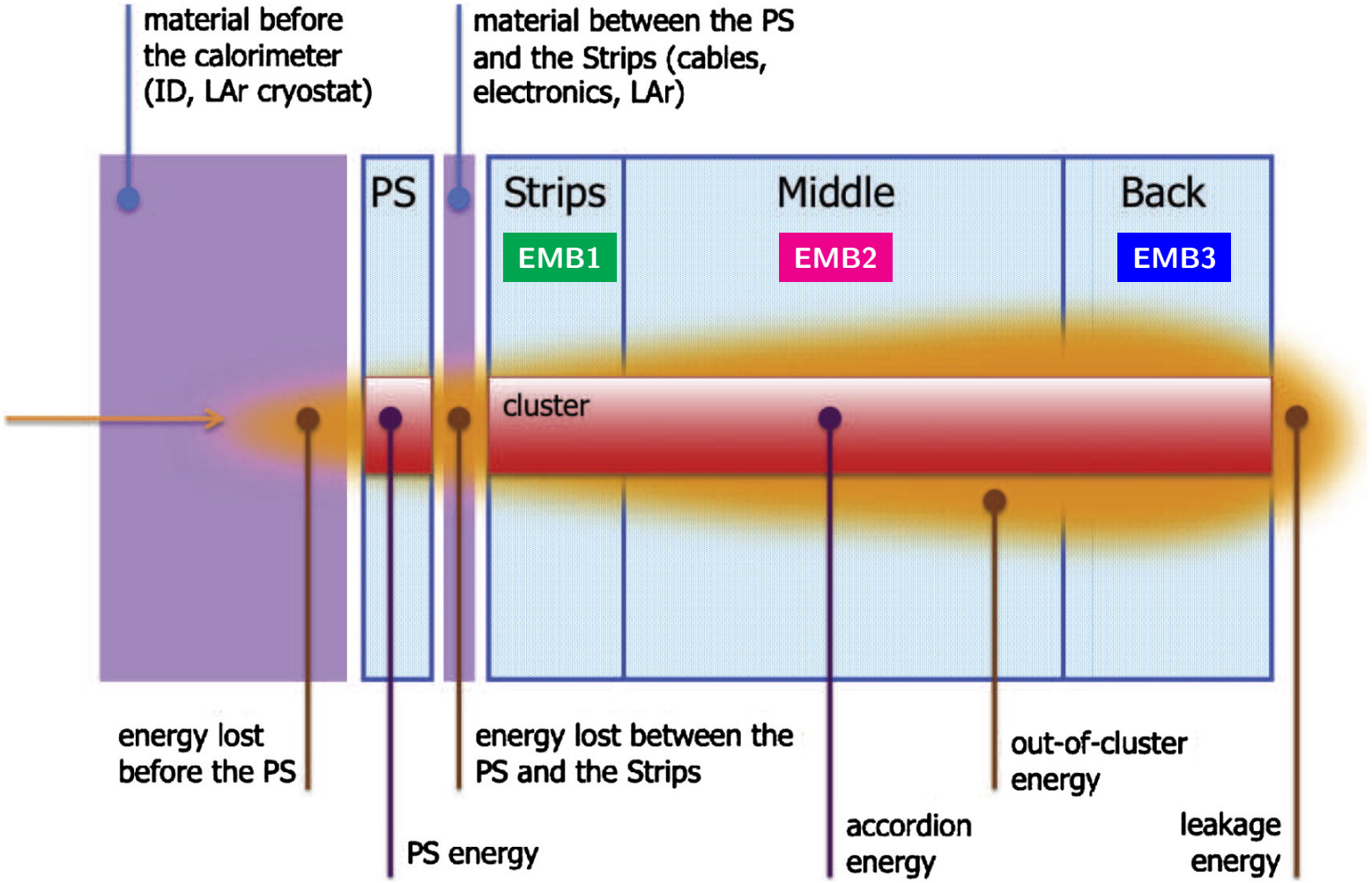

Energy reconstruction: cell energy

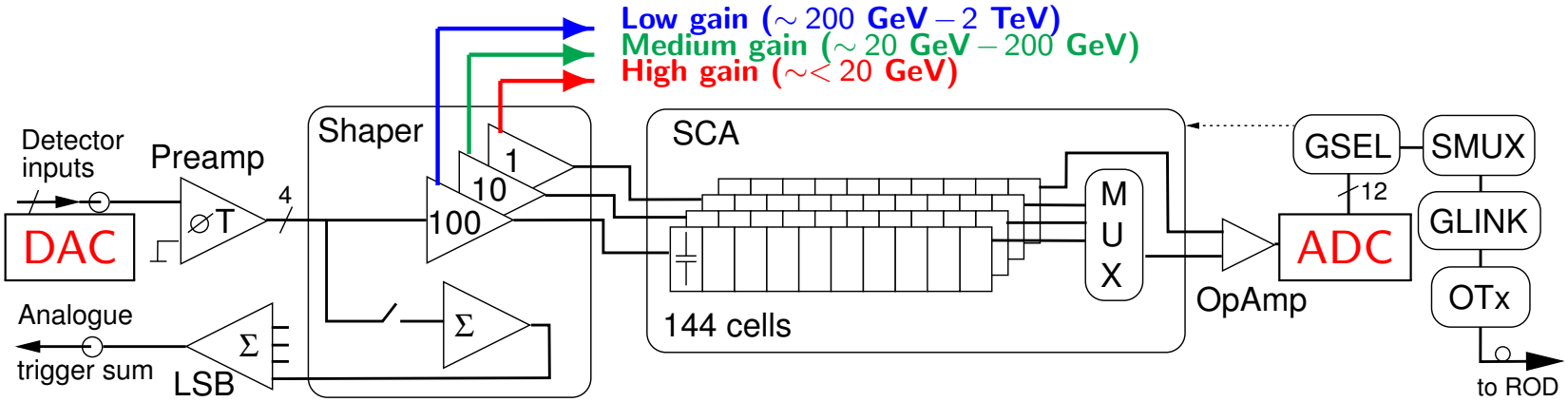

$$E = F_{\mu A \to MeV} \times F_{DAC \to \mu A} \times \frac{1}{\frac{M_{phys}}{M_{cali}}} \times \sum_{j=(0,1)}^{N_{ramps}} G_j A^j$$

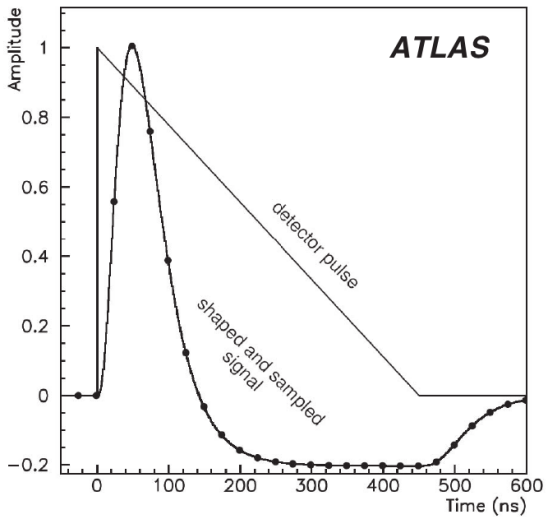

$F_{\mu A \to MeV}$: **ionization current to energy deposited.**

$F_{DAC \to \mu A}$: **DAC setting to the injected current.**

$\frac{M_{phys}}{M_{cali}}$: **ratio of response to a calibration pulse and an ionization pulse.**

G_j : **electronic gain.**

N_{ramps} : **order of polynomial function used to determine G_j.**

DAC: Digital-to-Analog Converter, ADC: Analog-to-Digital Converter.

Energy reconstruction: cell energy

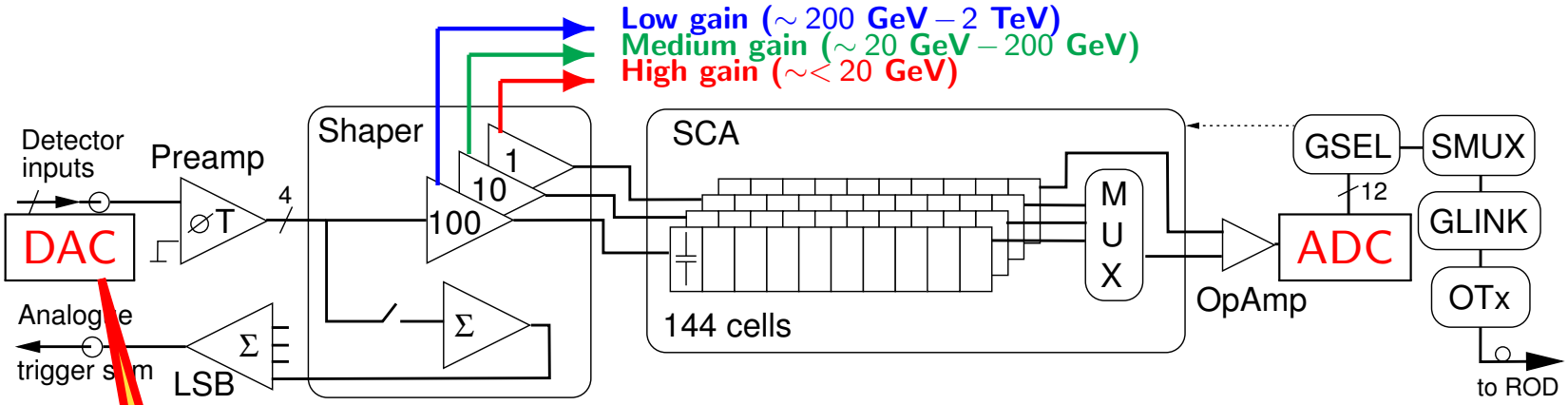

$$\mathbf{E = F_{\mu A \to MeV} \times F_{DAC \to \mu A} \times \frac{1}{\frac{M_{phys}}{M_{cali}}} \times \sum_{j=(0,1)}^{N_{ramps}} G_j A^j}$$

The calibration board injects current pulses of known amplitude on the detector cell, in order to probe the actual electronic response

- $\mathbf{F_{\mu A \to MeV}}$: **ionization current to energy deposited.**
- $\mathbf{F_{DAC \to \mu A}}$: **DAC setting to the injected current.**
- $\mathbf{\frac{M_{phys}}{M_{cali}}}$: **ratio of response to a calibration pulse and an ionization pulse.**
- $\mathbf{G_j}$: **electronic gain.**
- $\mathbf{N_{ramps}}$: **order of polynomial function used to determine G_j.**

DAC: Digital-to-Analog Converter, ADC: Analog-to-Digital Converter.

Energy reconstruction: electronic gains

Ramp fit: $\mathrm{DAC} = G_1 \cdot \mathrm{ADC} + G_0$

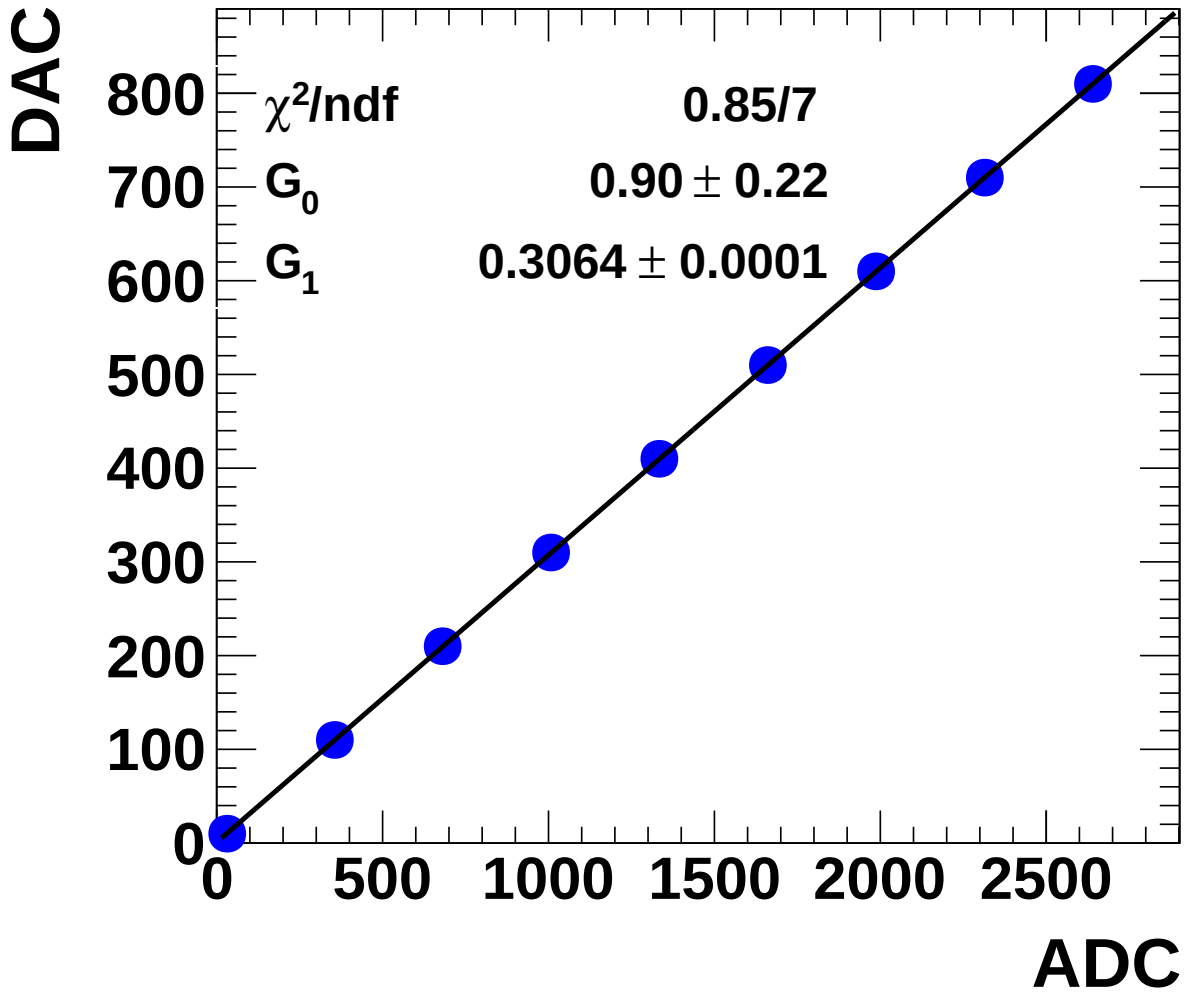

Effect of lost DAC on ramp fits

Motivation:

At the beginning of the data taking in 2009-2010, some errors occured during data recording where one of DAC values was not recorded $\to$ taking two ramp runs instead of one $\to$ take time!

$\to$ My study was to quantify the effect of lost DAC values.

- If the effect of lost DAC values is below $\sim 0.1\%$
  $\to$ the 2^{nd} ramp run is not needed.
- If a larger effect is observed
  $\to$ understand the effect and improve the stability of ramp fits.

Effect of lost DAC on ramp fits in high gain

- Comparing G_1 obtained from the ramp fit with full DAC values and without one DAC value: $\Delta_{G_1} = (G_1^{lost\_DAC} - G_1^{full\_DAC}) / G_1^{full\_DAC}$

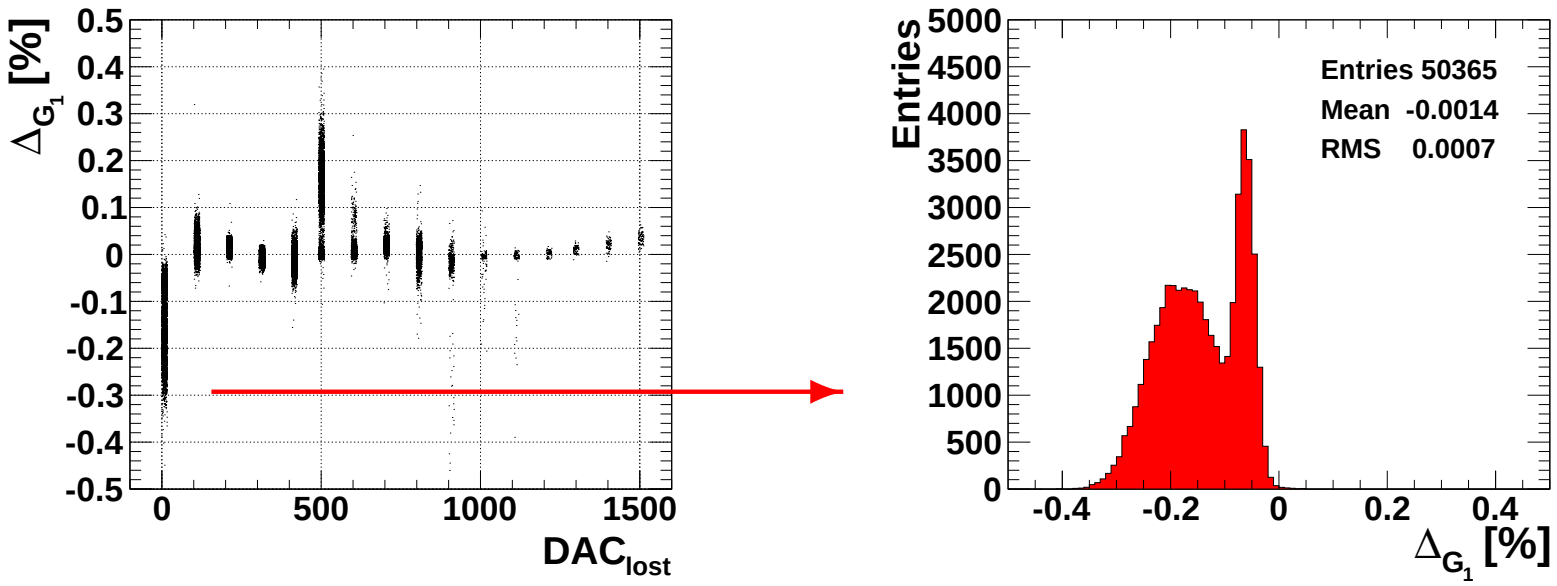

Observation: The effect of the lost DAC values is significant 0.2% for channels in EMB1.

Solution: Increase the number of DAC values in range $(0-500)$ for these channels to have more stable fits $\to$ has been applied.

Electron energy scale measurement

- Any residual miscalibration for a given region i in the EM calorimeter is parametrised by $E^{meas} = E^{true}(1+\alpha_i)$, α_i are energy scale correction factors.
- α_i are determined in following ways:

- Constrain the observed di-electron invariant mass distribution using $Z \to ee$ events.
- Cross check the result with E/p study, E measured by EM calorimeter, p measured by Inner Detector using $W \to e\nu$ events.

- Main systematic uncertainties: Material effect, presample detector energy scale, theoretical inputs (from the Z lineshape model).

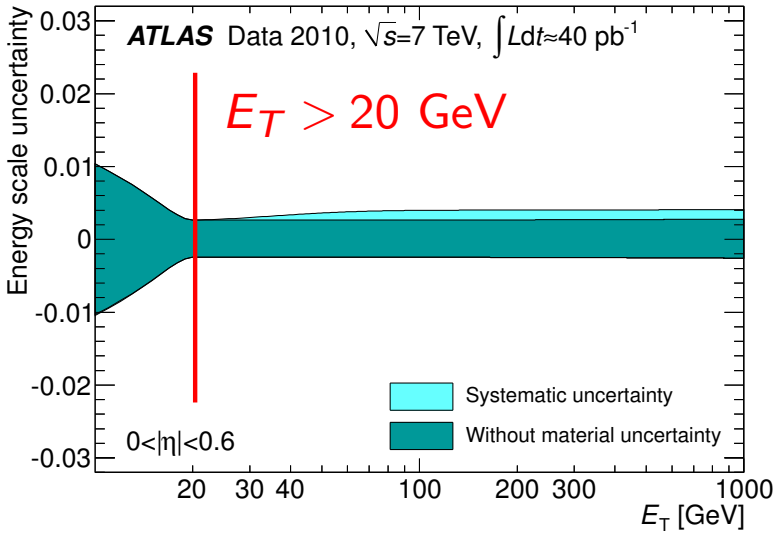

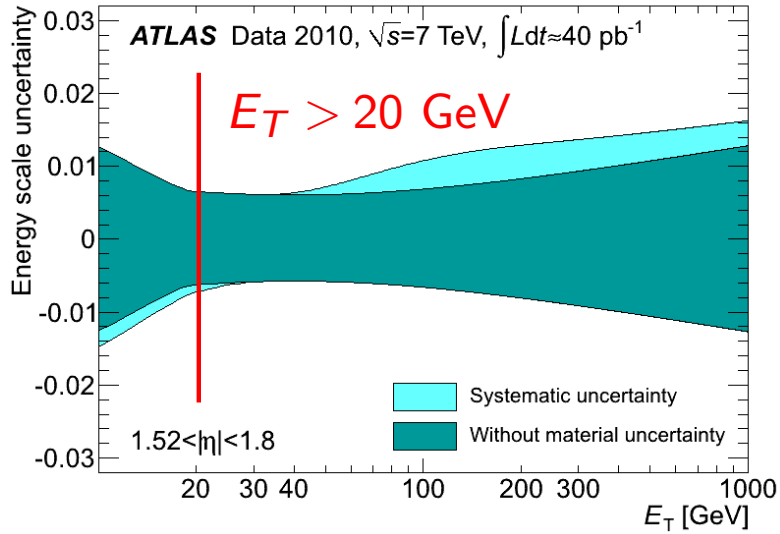

Electron identification efficiency measurement

- Electron identification criteria:

- Provide a good separation between signal electrons and background.
- Based on calorimeter and tracker information.

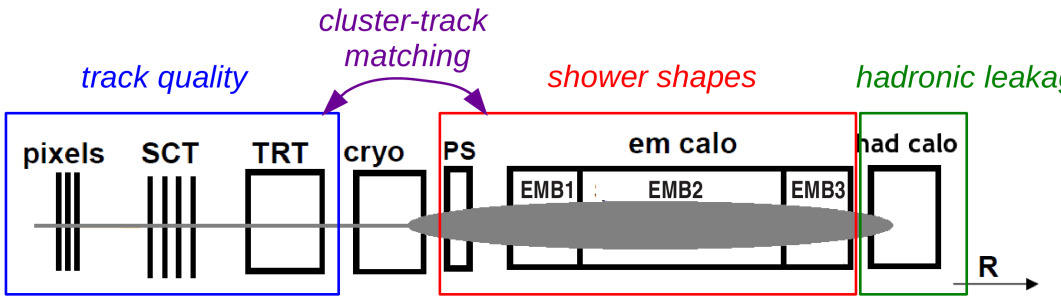

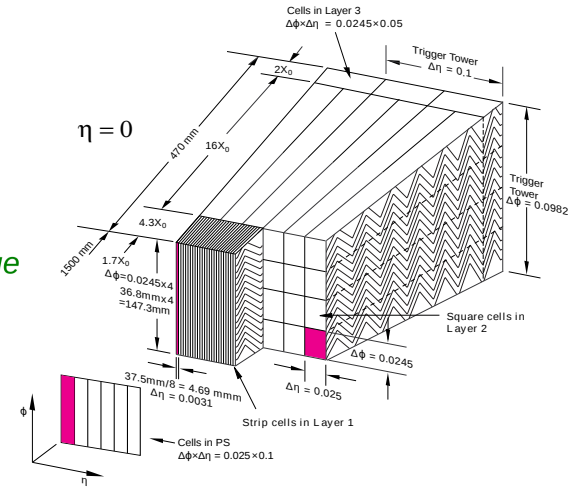

Identification	Selection efficiency [%]	Background rejection
Loose	95	~ 500
Medium	85	~ 5000
Tight	75	~ 50000

- Electron efficiencies are measured for both data and MC using the tag and probe method.

$Z \longrightarrow ee$ event reconstruction and background estimation

$Z \to ee$ event selection

Collision event selection	
Stable colliding beams + working detectors	
At least 1 good vertex	
Single electron trigger	$(E_T^{el} > 20(22)$ GeV$)$
Good electron selection	
Phase space	$p_{\mathrm{T}}^{el1} > 25$ GeV, $p_{\mathrm{T}}^{el2} > 20$ GeV
	$\lvert\eta_{trk}\rvert < 2.4$ excluding $1.37 < \lvert\eta_{cl}\rvert < 1.52$
Electron identification	Medium
$Z \to ee$ event selection	
2 highest p_{T} electrons	
Charge	Opposite sign
Invariant mass	66 GeV $< M_{ee} <$ 116 GeV

Electroweak background

Electroweak (EW) processes are well known
$\to$ EW background can be estimated from MC.

Sample	Process	$\sigma \times$ BR(nb)	Bck. fraction [%]
PYTHIA	$W \to e\nu$	10.5 ± 0.5	0.02
PYTHIA	$Z \to \tau\tau$	0.99 ± 0.05	0.05
MC@NLO	$t\bar{t}$	0.16 ± 0.01	0.12
HERWIG	WW	44.9×10^{-3}	0.16
HERWIG	ZZ	6.0×10^{-3}	
HERWIG	WZ	18.5×10^{-3}	

- The total fraction of EW background is 0.34%.
- Uncertainty of 10% on the contribution of EW background as a function of ϕ^*_η (p_T^Z) is assumed to propagate the systematic uncertainty in the final differential cross sections.

Multi-jet background

- Multi-jet cross section is large and not well known

→ difficult to estimate using MC

→ estimated from data using orthogonal selections with the signal.

- Two multi-jet background samples are used to estimate the systematic uncertainty as a function of ϕ^*_η (p_T^Z):
  - "Loosened ID template": using di-photon "loose" trigger.
  - "Non-isolated template": using non-isolation requirement (based on E_T^{cone}/E_T^{el})

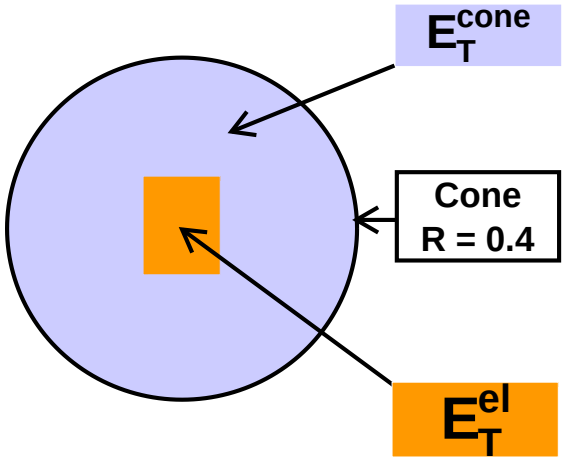

where $R = \sqrt{\Delta\eta^2 + \Delta\phi^2}$

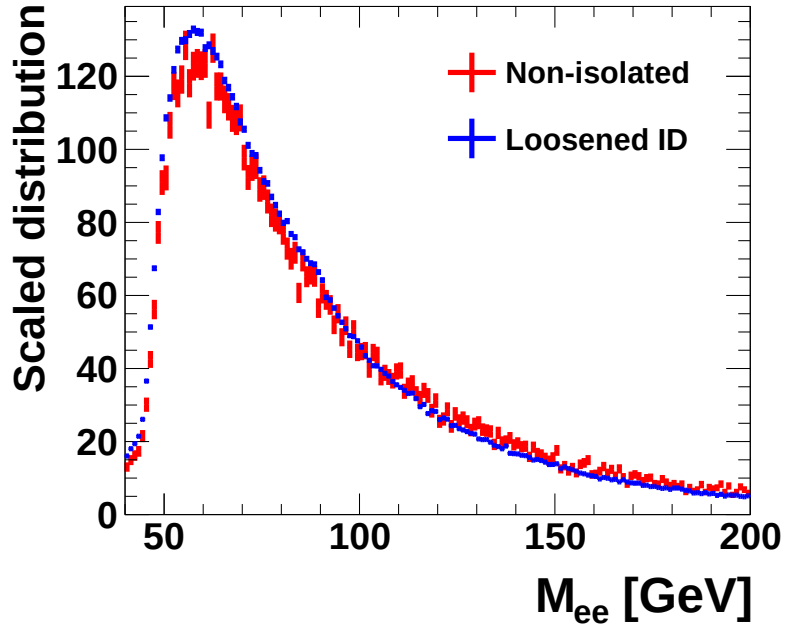

Multi-jet background: template fit

Method: using a binned likelihood fit on $Z \to ee$ mass distributions.

MC ⇓ from data ⇓

$$\mathbf{Data}(M_{ee}) = \mathbf{P_0} \cdot [\mathbf{Z} + \mathbf{EW}](M_{ee}) + \mathbf{P_1} \cdot \mathbf{QCD}(M_{ee})$$

→ The real multi-jet background (QCD) is estimated by scaling the background sample from data with parameter $\mathbf{P_1}$ from fitting results.

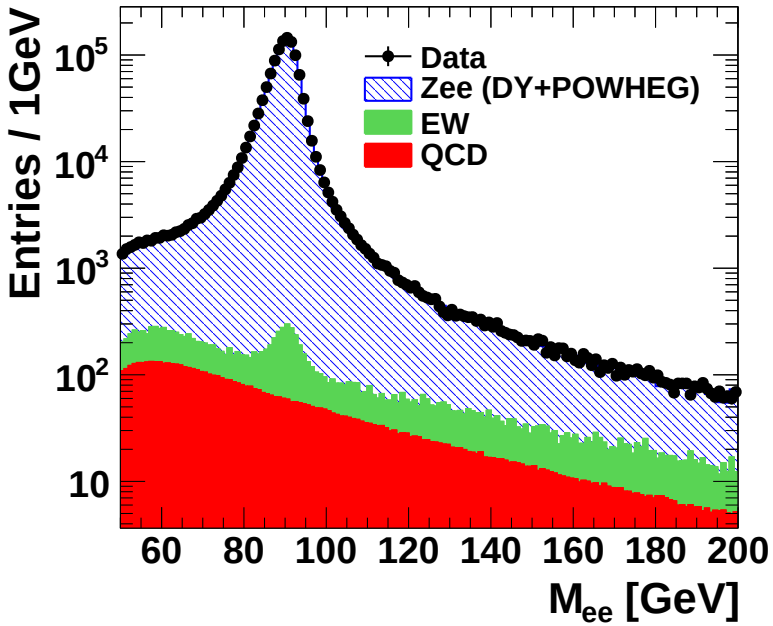

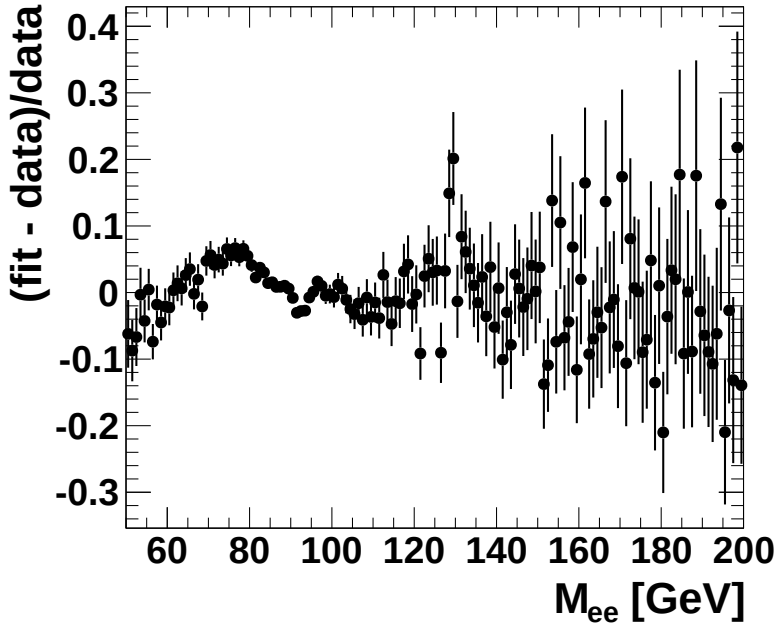

Multi-jet background

Systematic uncertainties: From template fit method

The nominal fit:

- The mass distribution with 1 GeV bin width.
- The fit range $[50, 200]$ GeV.
- The signal template of

$Z \to ee$ POWHEG+PYTHIA6 + low mass Drell-Yan samples.

$\to$ The fraction of multi-jet background is 0.27%.

Systematic uncertainty from the template fit method:

$\to$ Varying:

- The choice of fit ranges and bin widths.
- The choice of signal MC samples.

$\to$ Uncertainty of 47%.

Multi-jet background

Systematic uncertainties: From the choice of the multi-jet background samples

Only one selected multi-jet background sample may not describe perfectly the shape of this background in ϕ_η^* (p_T^Z).

$\to$ Use two independent samples to estimate the systematic uncertainty due to the choice of background samples.

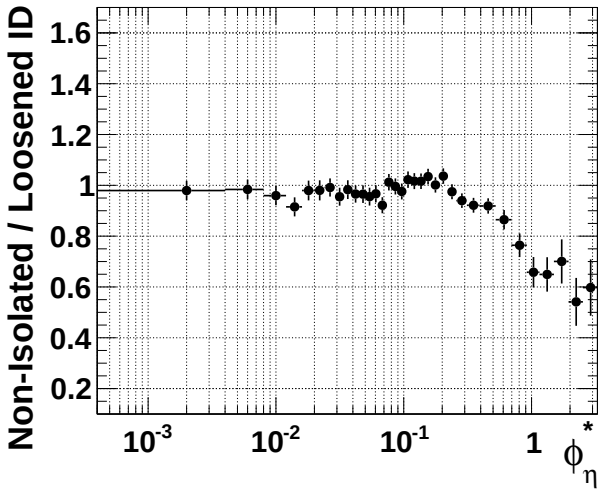

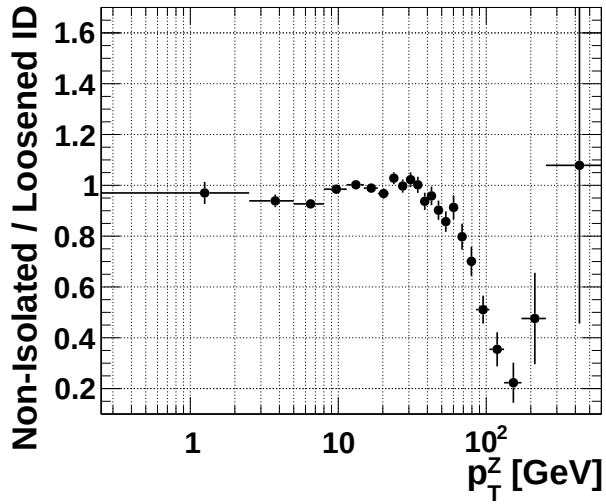

The difference between two samples as a function of ϕ_η^* (p_T^Z) is added in quadrature with the systematic uncertainty from the template fit method $\to$ used to propagate the systematic uncertainty in the final differential cross sections.

Selected data and MC sample results

Sample	Data	Prediction tot.	Diff. [%]
# candidates	1223711	1235240	0.9
Stat. Error	$\pm$1106	$\pm$573	

Sample	QCD	$Z \to ee$	$W \to e\nu$	$Z \to \tau\tau$	$t\bar{t}$	Diboson
# candidates	3256	1227771	222	643	1429	1919
Stat. Error	$\pm$6	$\pm$570	$\pm$16	$\pm$54	$\pm$26	$\pm$7

Control distributions

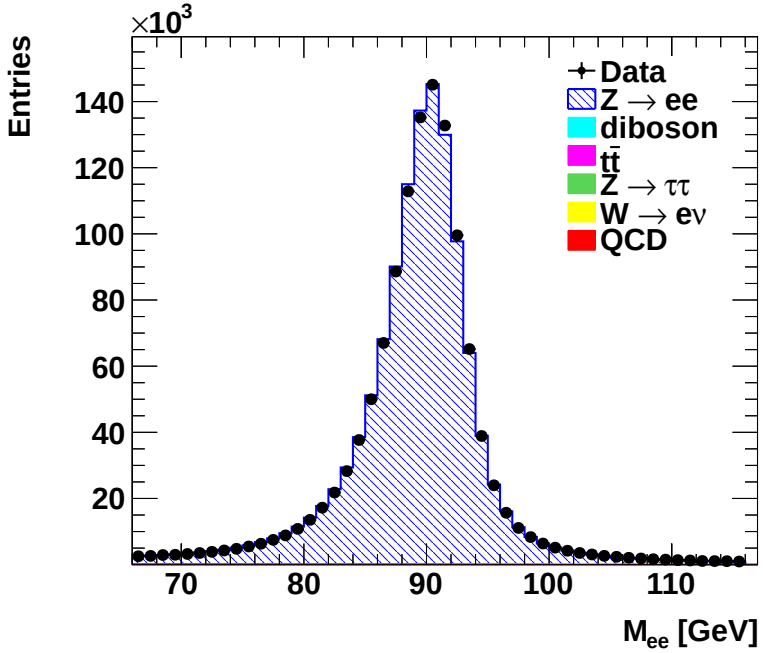

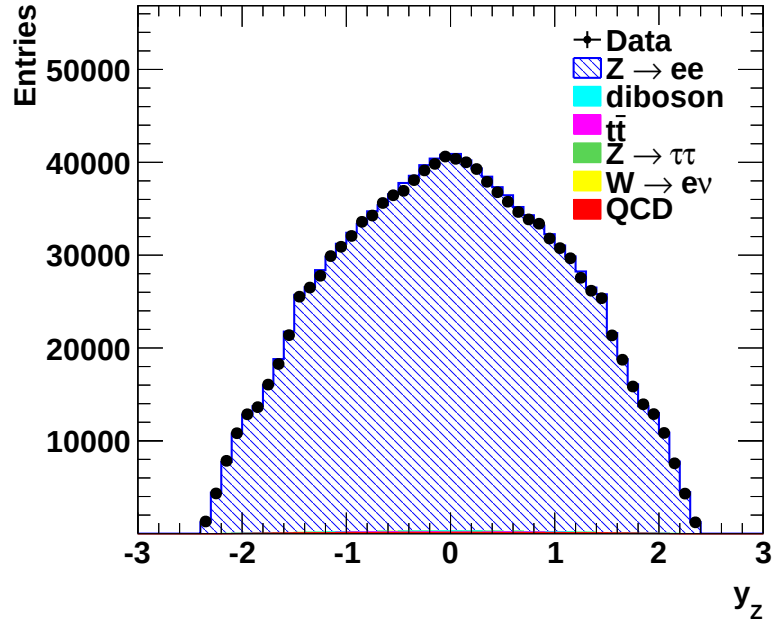

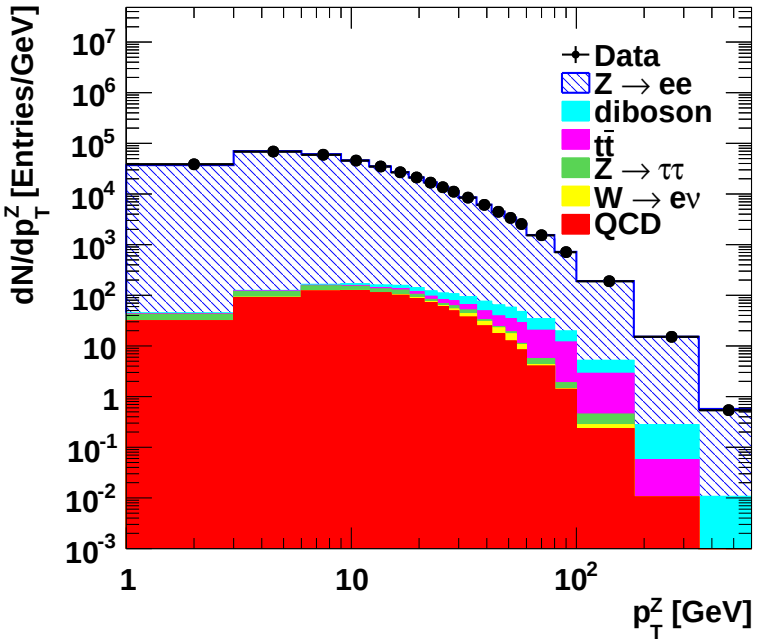

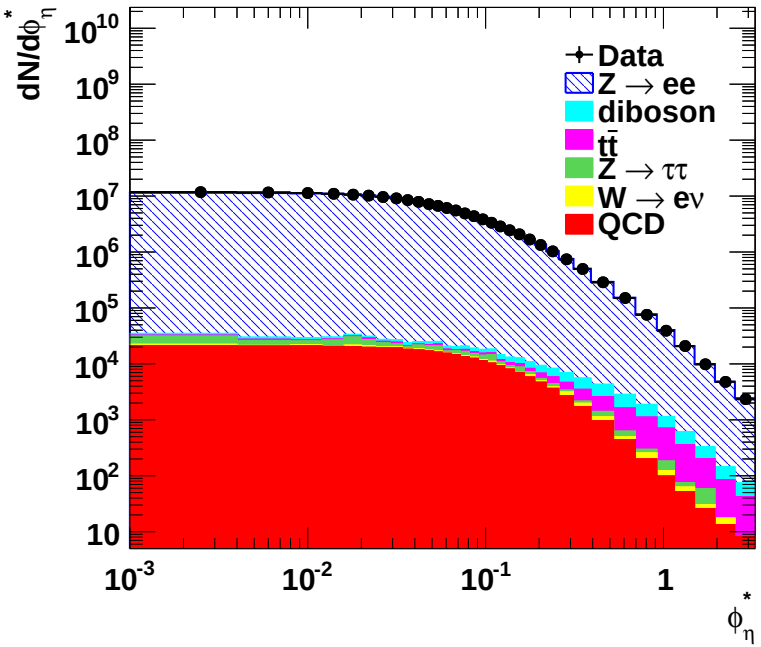

The differential cross section measurements

The differential cross section measurement of $Z \to ee$ as a function of ϕ^*_η (p^Z_T)

- The differential cross section: $\frac{1}{\sigma_{\text{fid}}} \cdot \frac{d\sigma_{\text{fid}}}{d\mathscr{R}}$, $\mathscr{R}$ is ϕ^*_η or p^Z_T.

- The cross section σ_{fid} is measured within the fiducial phase space: $p^{el}_T > 20$ GeV, $|\eta_{el}| < 2.4$, 66 GeV $< M_{ee} <$ 116 GeV.

- The measured ϕ^*_η (p^Z_T) spectrum is corrected for detector and QED final state radiation (FSR) effects using an unfolding technique to the underlying "true" spectrum.

- The "true" spectrum is defined at different reference points referring to the amount of QED FSR corrections considered at the generator level: "Born", "Dressed", "Bare".

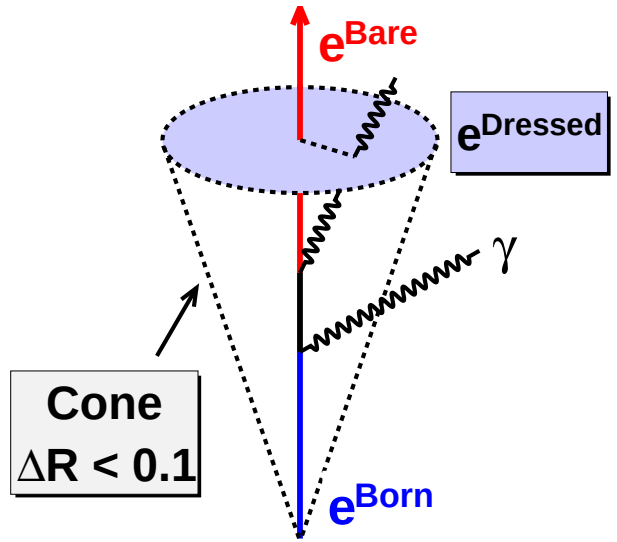

Purity and binning

$$\text{Purity} = \frac{N_{\text{reconstructed and true parameter in the same bin}}}{N_{\text{reconstructed parameter in the bin}}}$$

- Purity is used to optimize bin widths of the measurement.
- Purity is related to the event migration, higher purity corresponds with lower migration $\rightarrow$ control the unfolding procedure.

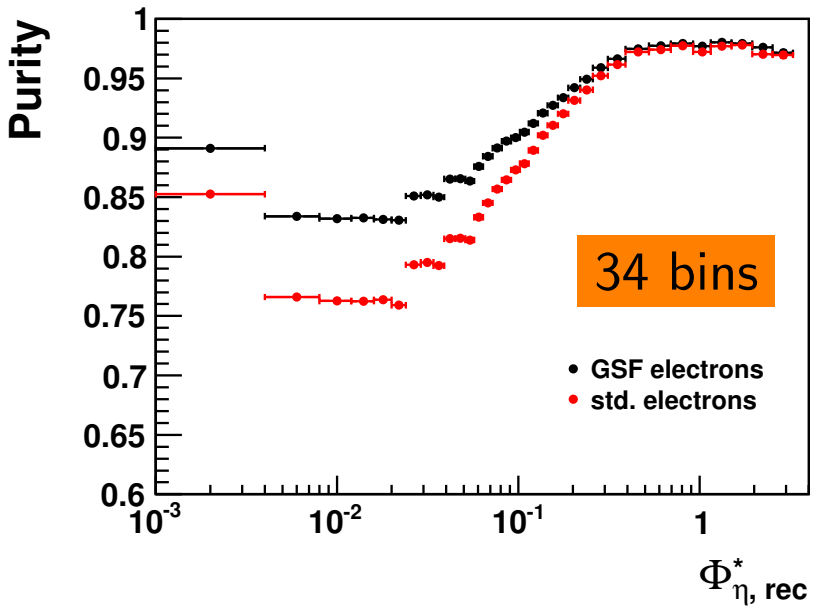

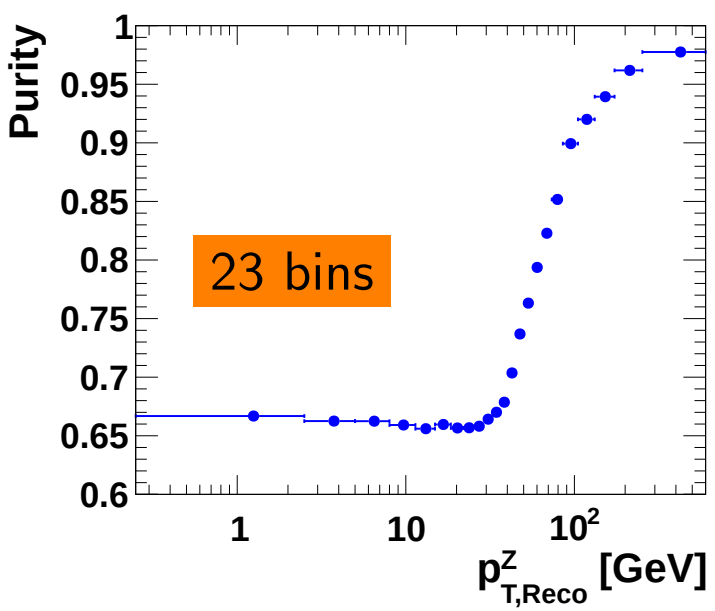

High purity using GSF electron is observed in the ϕ^{*}_{η} measurement.

Unfolding methods

Instead of measuring **x** one typically measures a related variable **y**: $\mathbf{y} = \mathbf{A}\mathbf{x}$, **A** is the response matrix describing detector effects.

Bin-by-bin unfolding:

$$\left(\frac{1}{\sigma}\right)_{fid}\left(\frac{\Delta\sigma_i}{\Delta\mathscr{R}_i}\right)_{fid} = \frac{C}{C^i}\cdot\frac{\left(N^i_{\text{data}} - N^i_{\text{bg}}\right)}{\Delta\mathscr{R}_i\cdot\left(N^{tot}_{\text{data}} - N^{tot}_{\text{bg}}\right)}$$

$$C^i = \frac{N^i_{\text{MC,rec,cuts}}}{N^i_{\text{MC,gen,fid}}} \quad , \quad C = \frac{N^{tot}_{\text{MC,rec,cuts}}}{N^{tot}_{\text{MC,gen,fid}}}$$

Iterative Bayesian unfolding:

$$\hat{\mu}_i = \frac{1}{\varepsilon_i}\sum_{j=1}^{m} p(t_i|o_j)\, n_j$$

Number of events in truth

Efficiency

$$p(t_i|o_j) = \frac{p(o_j|t_i)p_i}{\sum_{i=1}^{N} p(o_j|t_i)p_i}$$

Number of events observed

$p(o_j|t_i)$ is the response matrix and can be inferred from Monte Carlo.

Unfolding procedure

For the ϕ^*_η measurement: bin-by-bin correction factor to correct to "Born" level

$$C^i_{norm} = \frac{C^i}{C}$$

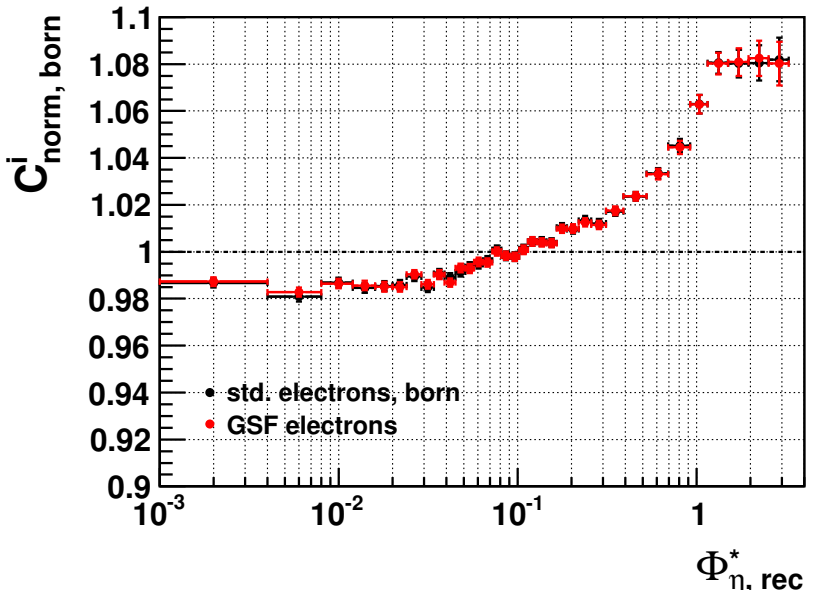

For the p^Z_T measurement: iterative Bayesian response matrix to correct to "Born" level

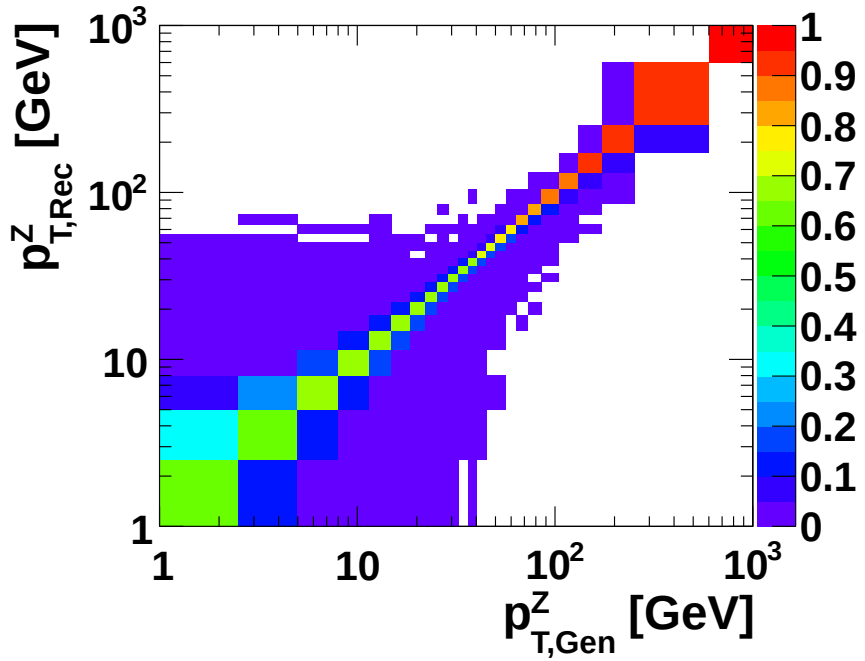

Evaluation of systematic uncertainties

$$X = 1/\sigma_{\text{fid}} \times d\sigma_{\text{fid}}/d\mathscr{R}$$

$$\mathrm{D} = \frac{X_{\text{systematic}} - X_{\text{central}}}{X_{\text{central}}}$$

In the case of energy scale, energy resolution, efficiency, background systematic uncertainties, the relative deviation (up and down) is propagated $\to$ the central systematic uncertainty value:

$$D = \text{sign} \cdot \frac{1}{2} \cdot \left[|D^{\text{up}}| + |D^{\text{down}}| \right]$$

$D^{\text{up}} > 0$: $\text{sign} = 1$
$D^{\text{up}} < 0$: $\text{sign} = -1$

All systematic uncertainties are added in quadrature
$\to$ The total systematic uncertainty of the measurement.

Main systematic uncertainties

- Other systematic uncertainties including pileup, $z-$vertex shape, electron efficiencies, backgrounds are small.
- Main systematic uncertainties:

Sys. unc.	ϕ^*_η	p^Z_T
Tracking	$< 0.3\%$	
Unfolding	$< 0.2\%$	$< 2.5\%$
Energy scale and energy resolution	$< 0.1\%$	$< 2.5\%$
QED final state radiation	0.3%	

A lot of work to get systematic uncertainties at the level of per mil for the ϕ^*_η measurement!

Systematic uncertainties: Tracking

Angular resolution

The effect of a possible mis-description of the detector resolution on the measurements of ϕ and η angles has also been studied.

$\to$ The resolution in the MC on both angles is increased by 50%.

$\to$ A change of the resolution on η has no impact on the measured cross section. A change of the resolution on ϕ has a maximal effect of 0.2%.

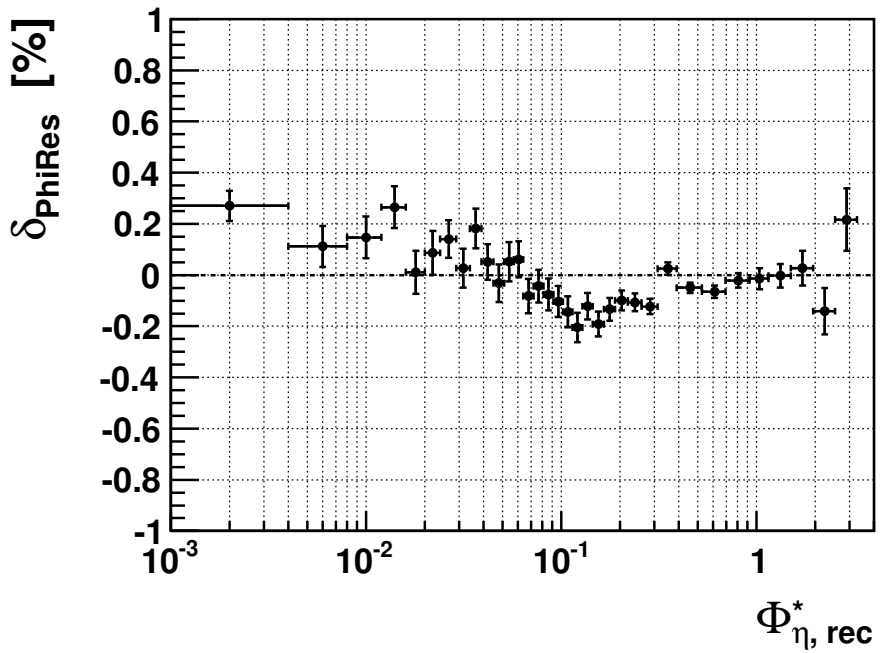

Systematic uncertainties: Unfolding

- Use $Z \to ee$ MC sample reweighted to different truth spectra obtained from the RESBOS prediction or from "data" for the unfolding procedure.

(MC reweighted to "data": unfold the ϕ^*_η (p^Z_T) distribution in data using default MC $\to$ use the unfolded ϕ^*_η (p^Z_T) distribution to reweight MC)

- $Z \to ee$ MC sample reweighted to "data" is used for the central result other samples are used for the systematic uncertainty study.

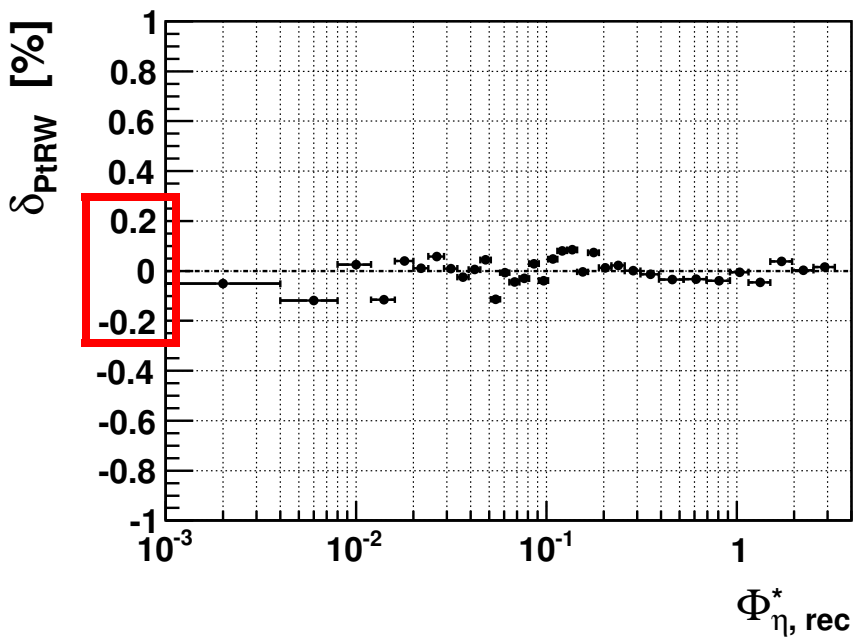

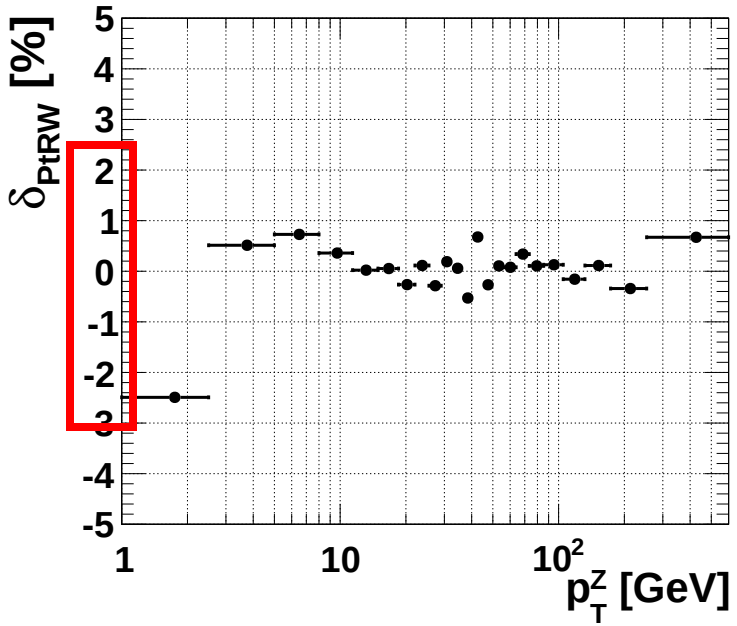

Systematic uncertainties: Energy scale

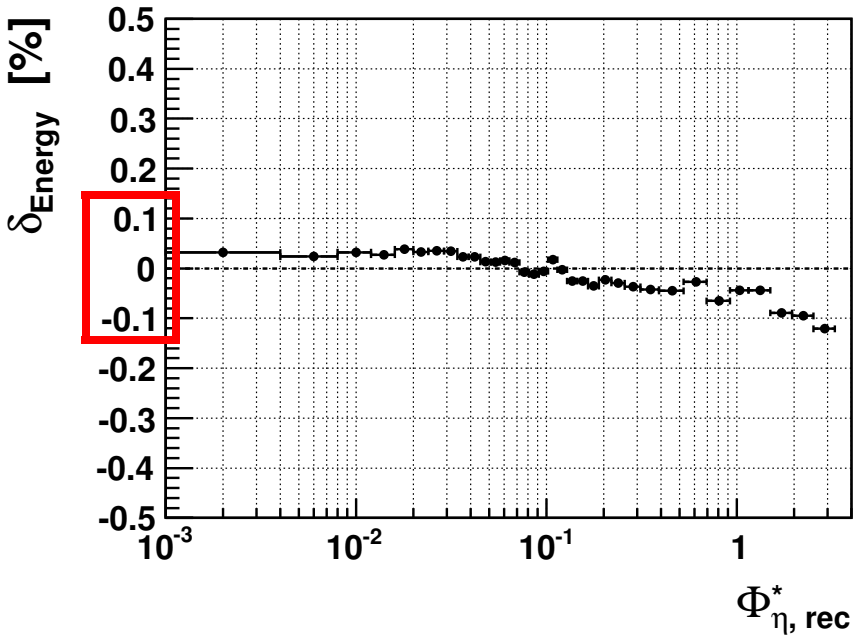

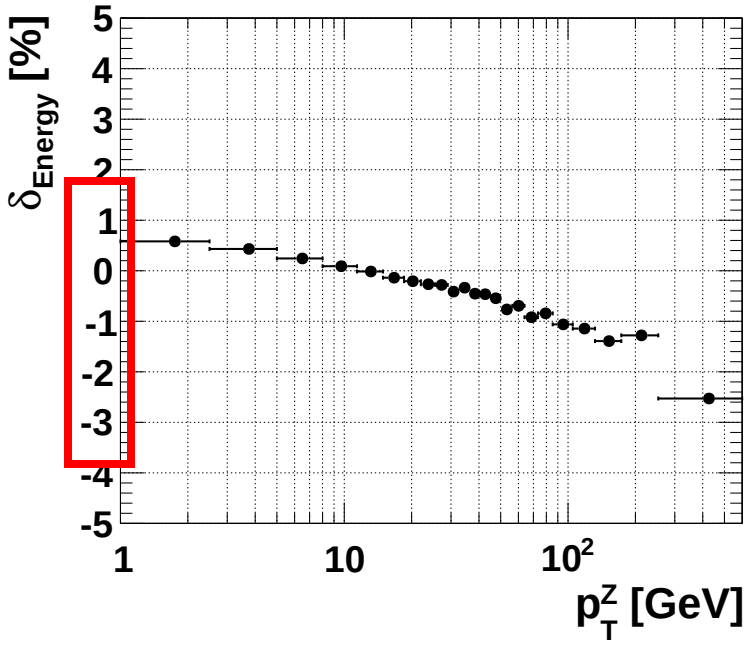

Energy scale uncertainty in the ϕ^*_η measurement is small as expected.

Systematic uncertainties: QED FSR (1/2)

- $Z \to ee$ POWHEG+PYTHIA6 (reference signal MC sample) uses PHOTOS to simulated QED FSR
(PHOTOS is a process-independent module for adding multi-photon emission)

- $Z \to ee$ SHERPA uses YFS formalism to simulated QED FSR
(YFS-resummation of soft logarithms for QED radiation)

$\to$ Compare $Z \to ee$ POWHEG+PYTHIA6 with $Z \to ee$ SHERPA

- To extract pure QED FSR effect:

$$\mathrm{QED}_{\mathrm{Bare}} = \frac{\left(\left(\frac{1}{\sigma}\right)_{fid}\left(\frac{\Delta\sigma_i}{\Delta\phi^*_{\eta\,i}}\right)_{fid}\right)_{\mathrm{Bare}}}{\left(\left(\frac{1}{\sigma}\right)_{fid}\left(\frac{\Delta\sigma_i}{\Delta\phi^*_{\eta\,i}}\right)_{fid}\right)_{\mathrm{Born}}}$$

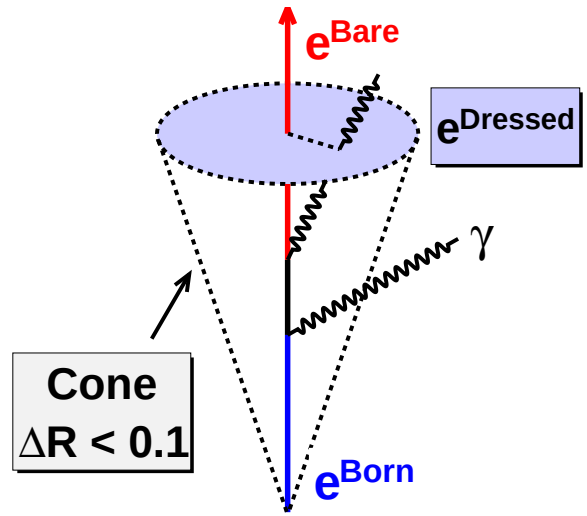

Systematic uncertainties: QED FSR (2/2)

- To extract systematic uncertainty:

$$(\mathrm{QED}_{\mathrm{Bare}})_{\mathrm{POWHEG+PYTHIA6}} \Big/ (\mathrm{QED}_{\mathrm{Bare}})_{\mathrm{SHERPA}} - 1$$

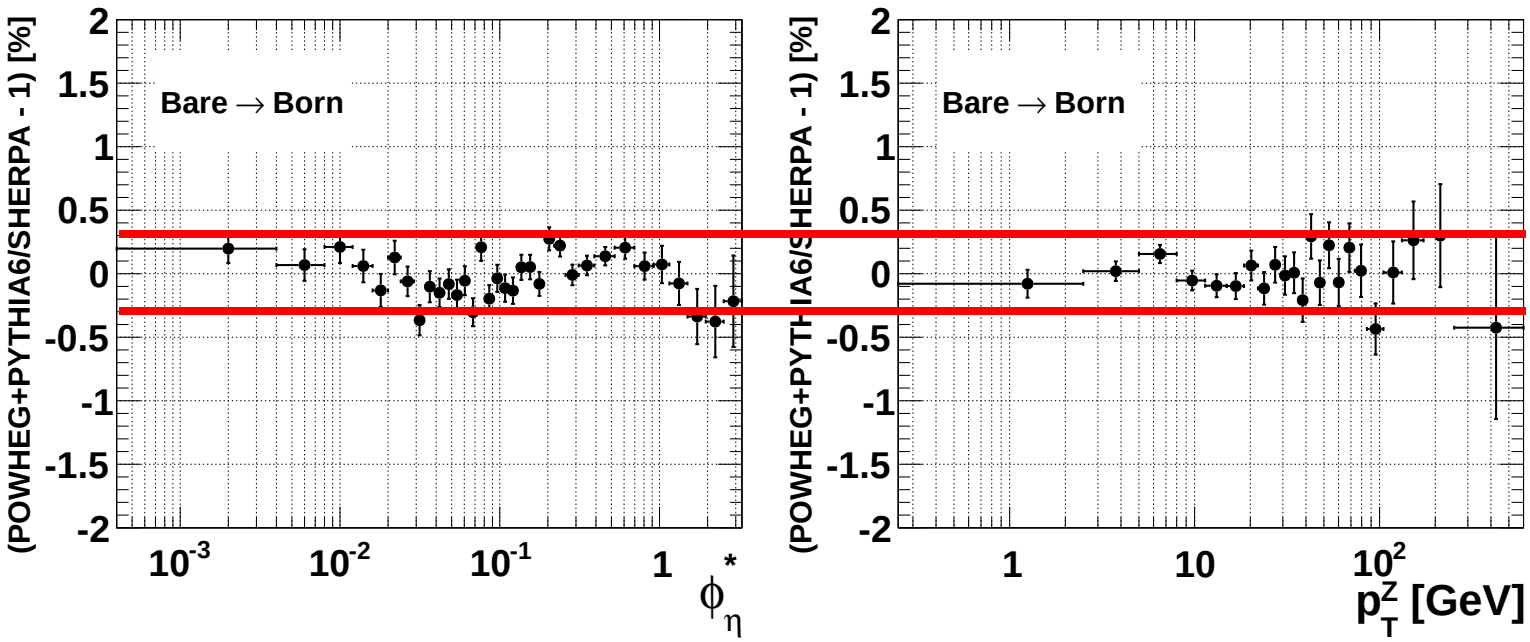

→ Uncertainty of 0.3% for ϕ^*_η (p_T^Z) distributions at the "Born", "Dressed" and "Bare" levels.

(This conclusion was discussed with the authors of PHOTOS.)

The unfolded differential cross section: ϕ^*_η

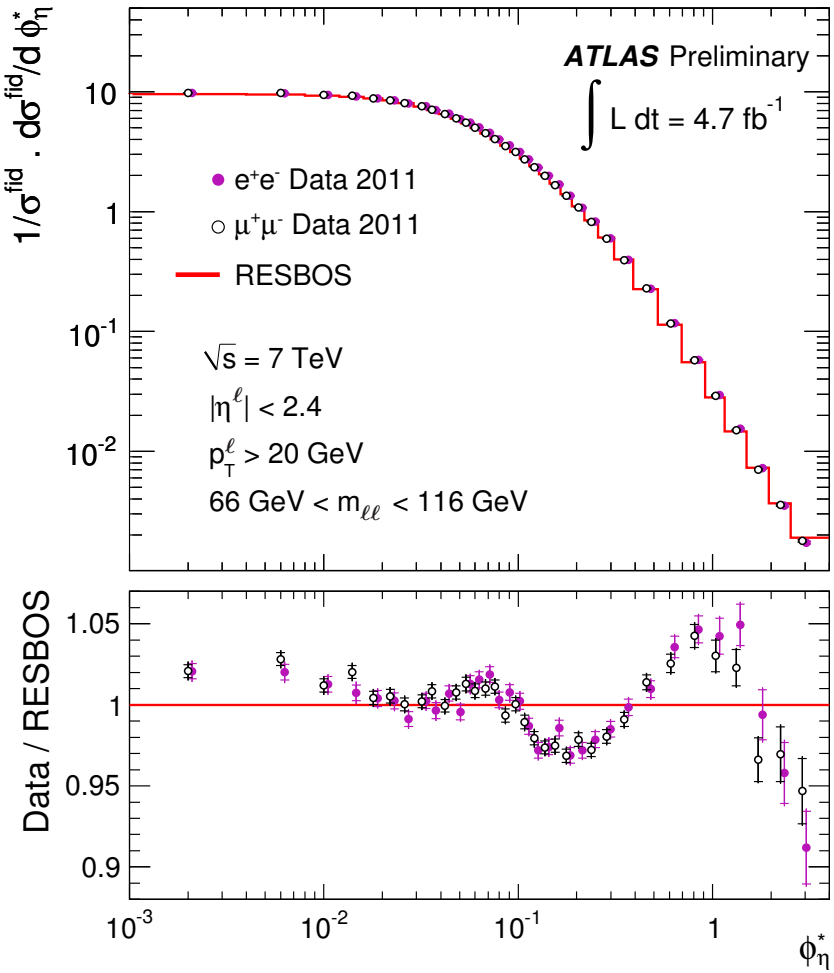

- Statistic uncertainty: $0.5 - 2.5\%$
- Systematic uncertainty: $\sim 0.5\%$ in most of the ϕ^*_η range.
- Agree with RESBOS CT10 within 3% at low ϕ^*_η and within 5% at high ϕ^*_η as observed in the ϕ^*_η measurement by D0.

Comparison with QCD predictions

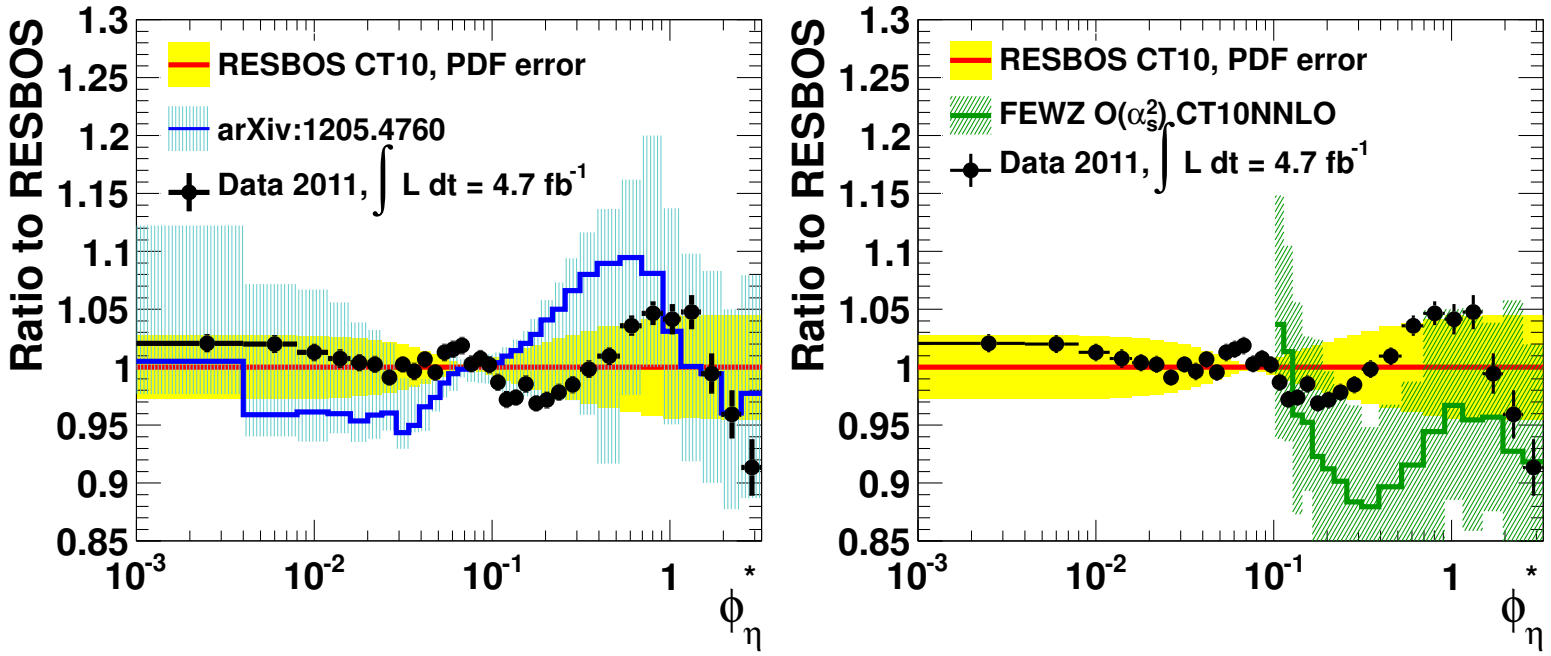

- New prediction: NLO prediction + resummation for the low ϕ_η^* region (arXiv:1205.4760).
- FEWZ: NNLO predictions without resummation.

- Better agreement with RESBOS than with NNLO FEWZ and NNLL+NLO prediction from Ref.[arXiv:1205.4760].
- Difference between data and RESBOS prediction is covered by PDF uncertainty.

Comparison with MC generator predictions

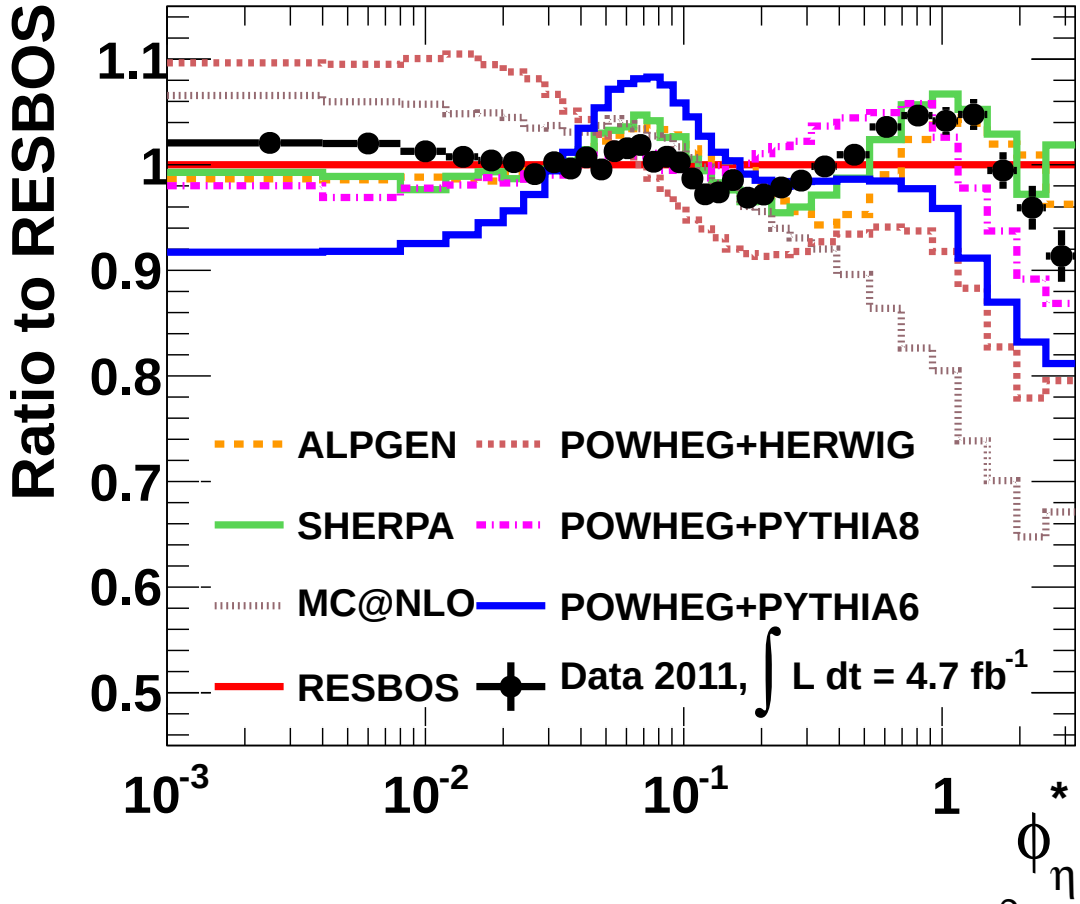

- The best description is provided by SHERPA based on χ^2 test.
- POWHEG+HERWIG, POWHEG+PYTHIA6 can not describe data while POWHEG+PYTHIA8 has a certain agreement.
- MC@NLO (interfaced with HERWIG) underestimate data at high ϕ^*_η.

$\to$ This precise measurement can be used to tune MC for future studies.

The unfolded differential cross section: p_T^Z

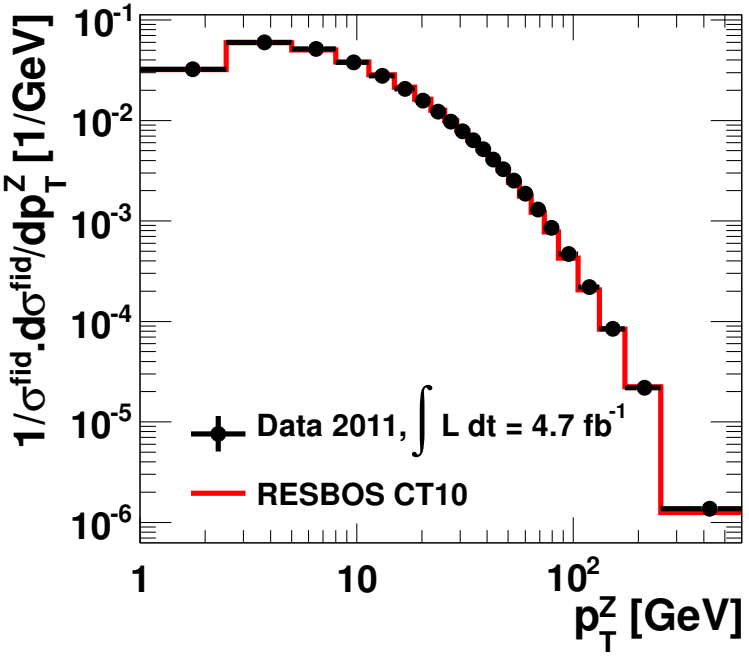

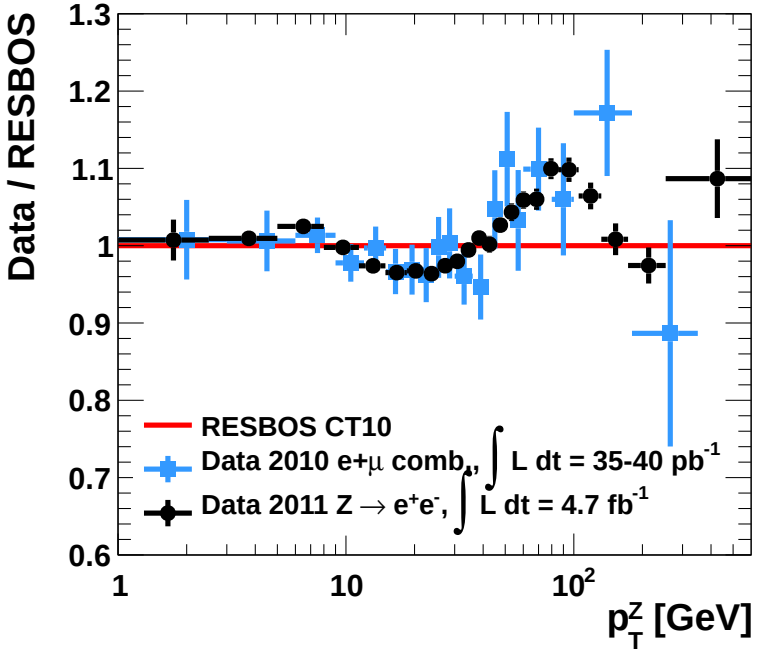

- Statistic uncertainty: $0.2 - 1.9\%$ (last bin 3.6%)
- Systematic uncertainty: $\sim 1\%$, first bin 2.6%, last bin 3%.

- The result of the p_T^Z measurement in this analysis using 4.7 fb^{-1} shows a good agreement with the p_T^Z measurement published by ATLAS using $35 - 40$ pb^{-1} (Phys. Lett. B, 705:415434, 2011.) (systematic uncertainty of $\sim 2\%$, first bin 4.7%, last bin 5.4%).

ϕ^*_η and p^Z_T comparison

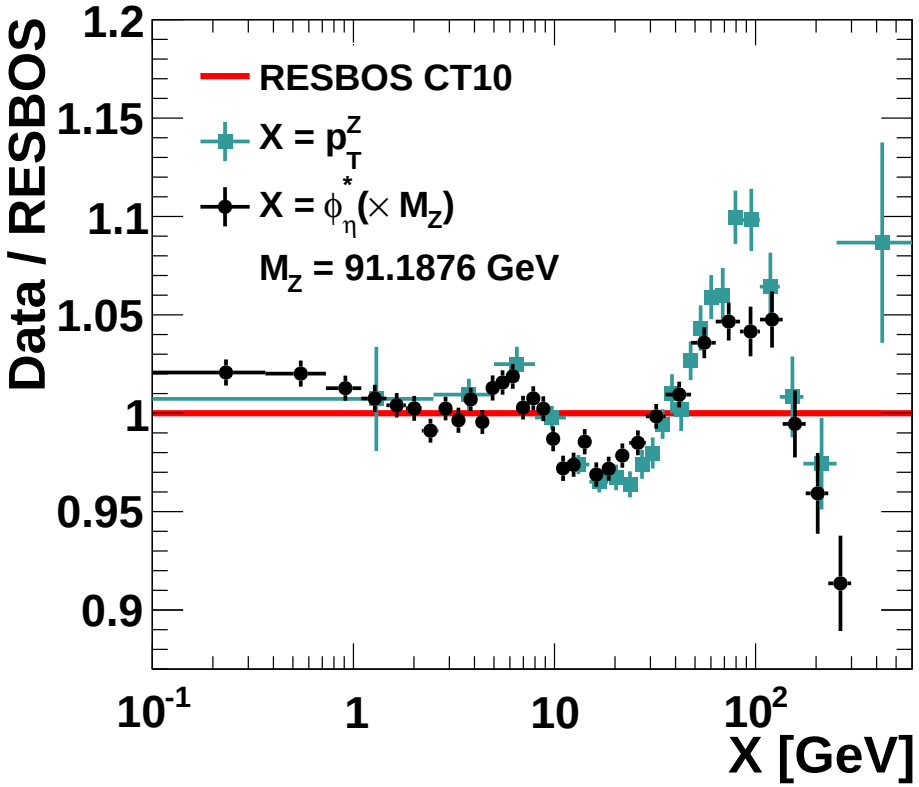

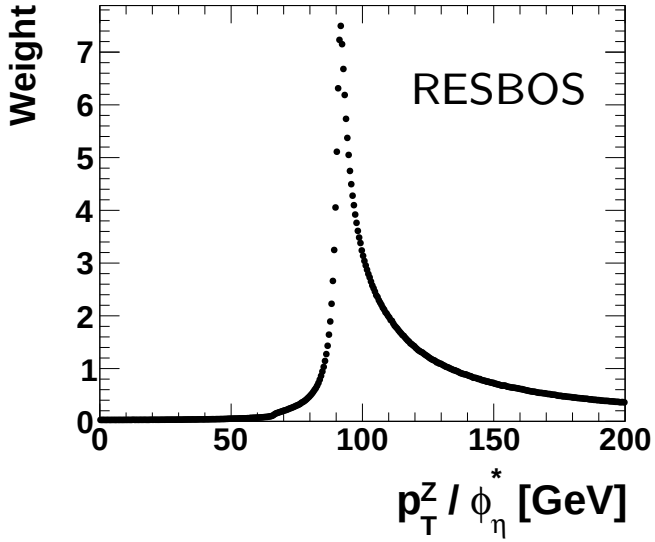

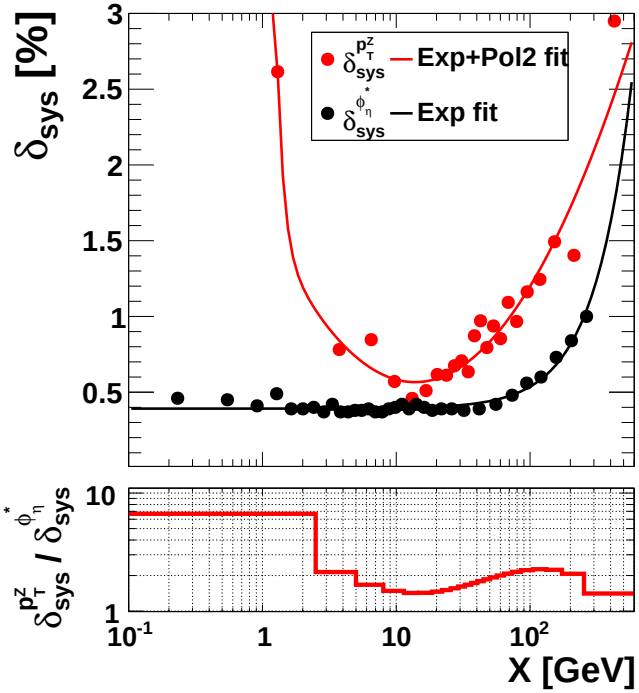

At $p^Z_T < 10$ GeV:

- Both measurements agree with the predictions within 3%.
- The p^Z_T measurement only can be split in three bins due to the limit of the p^Z_T resolution.
- The ϕ^*_η measurement can result the shape with more than ten bins.

Conclusion

The first measurement of the ϕ^*_η spectrum of Z bosons at $\sqrt{s} = 7$ TeV of pp collisions using the full 2011 ATLAS data sample corresponding with 4.7 fb^{-1} integrated luminosity.

- At low ϕ^*_η ($\phi^*_\eta < 0.1$): agree with RESBOS CT10 within 3%.
- At high ϕ^*_η: better agreement with RESBOS CT10 than with NNLO FEWZ and NNLL+NLO prediction from Ref.[arXiv:1205.4760].
- Among MC generators: the best description by SHERPA. MC@NLO, POWHEG+HERWIG, POWHEG+PYTHIA6 underestimate the data at higher ϕ^*_η.
- The typical experimental precision ($\sim 0.5\%$) is now ten times better than the typical theoretical precision and therefore is valuable to constrain the theoretical predictions further.

The results were reported in ATL-COM-PHYS-2012-472 and in conferences. The public paper is in the last state of the approval (CERN-PH-EP-2012-325).

Thank you!

Detailed contents

Detailed contents

The muon spectrometer

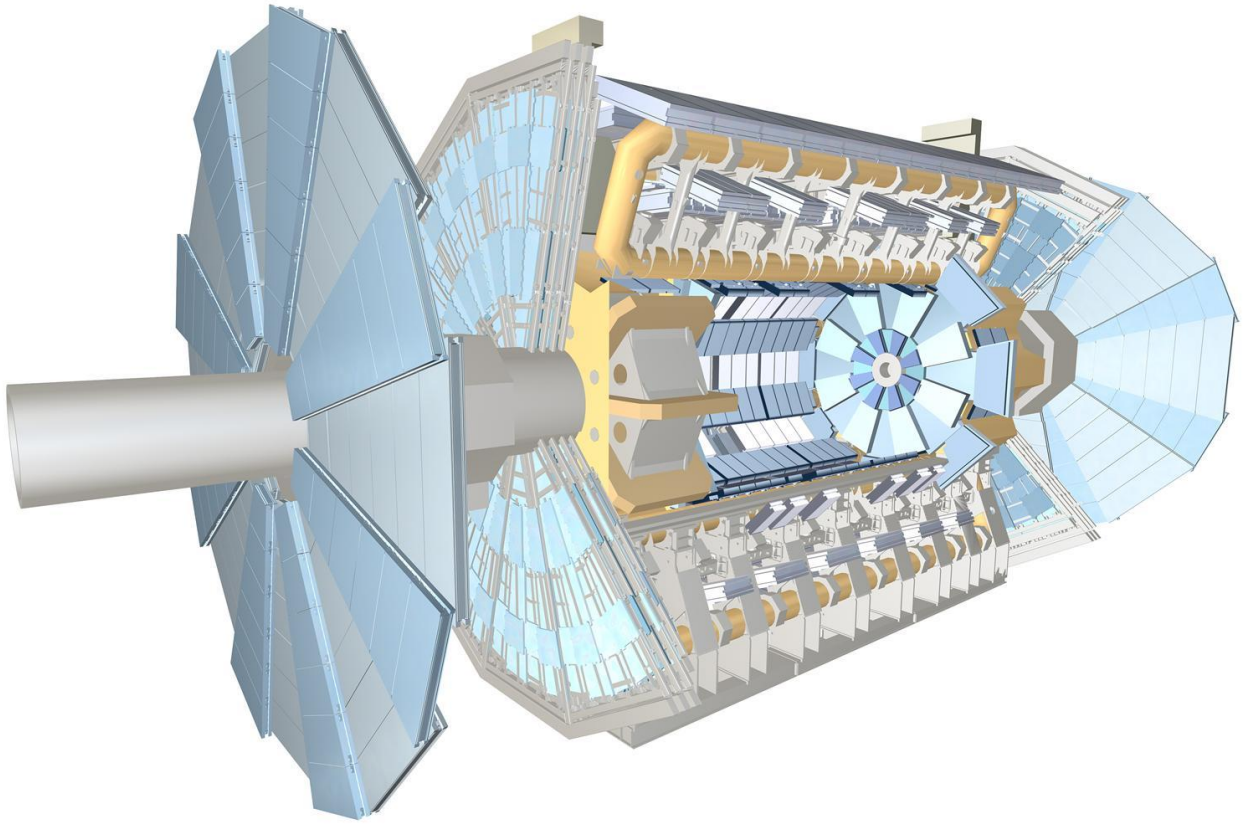

Required resolution	η coverage
$\sigma_{p_T}/p_T = 10\%$ at $p_T = 1\,TeV$	± 2.7

The magnet system

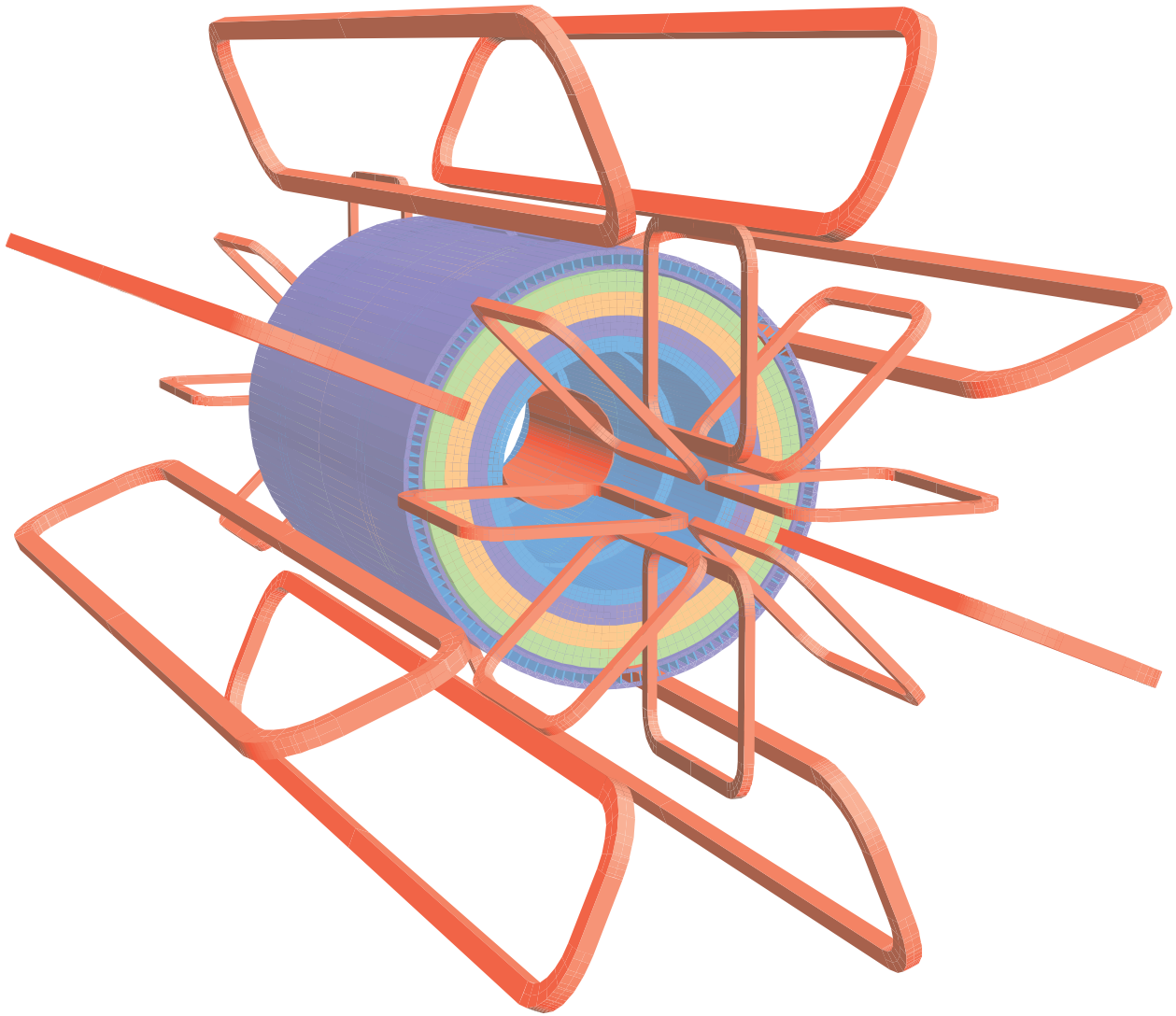

The Trigger system

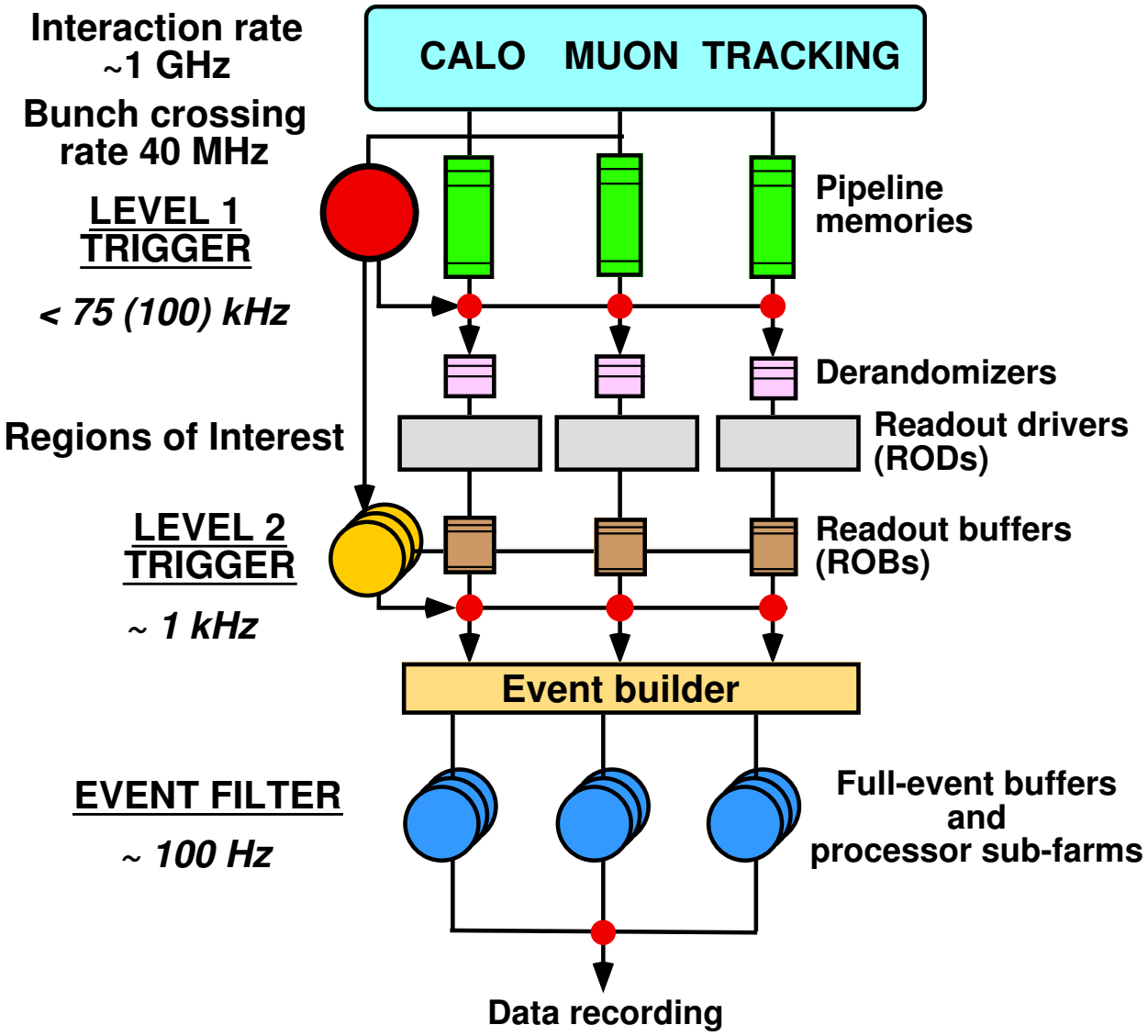

Fitting using 3 ϕ_η^* range samples

DY+POWHEG 1 GeV bin [50, 200]

Procedure	QCD Fraction [%]	Fit Error [%]	Stat. unc [%]
Nominal value	0.27	6.60	0.17
$\phi_\eta^* < 0.05$	0.30	9.04	0.31
$0.05 < \phi_\eta^* < 0.3$	0.25	10.32	0.23
$\phi_\eta^* > 0.3$	0.24	20.84	0.43

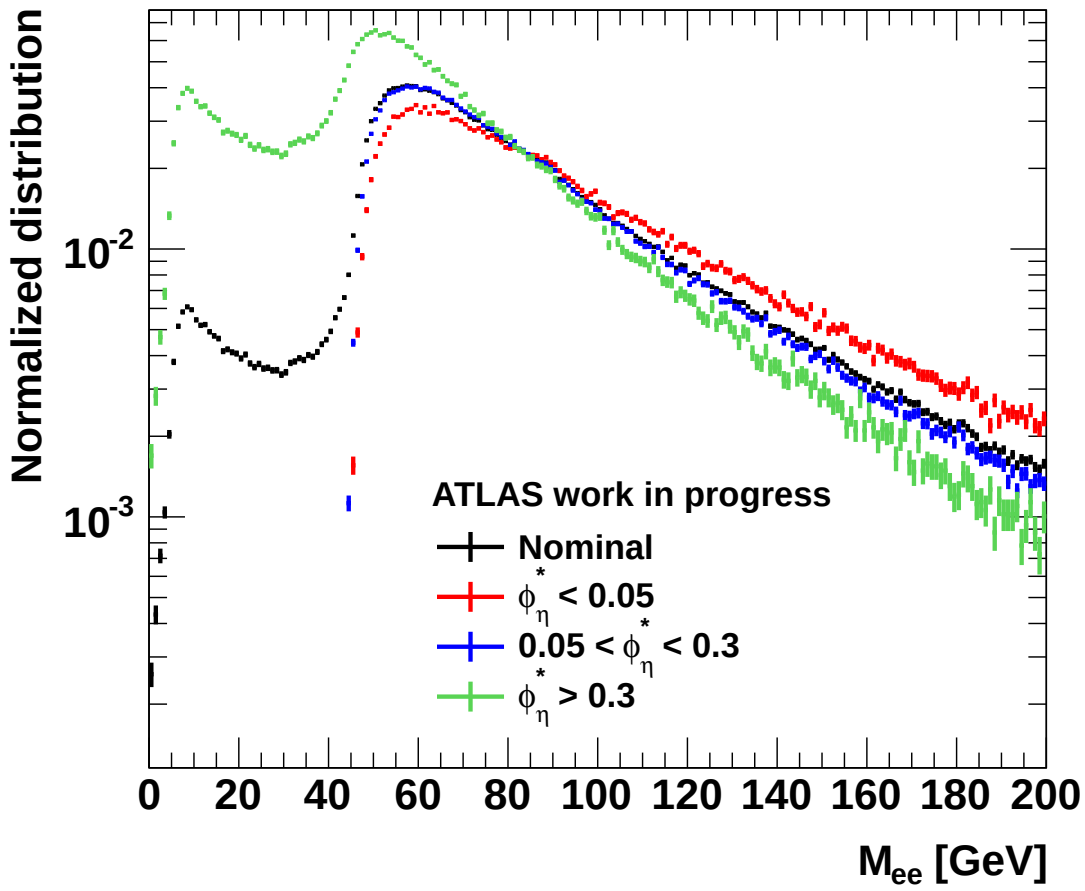

QCD fraction in each ϕ^*_η bin

Bin	Range	Syst. unc. [%]	QCD fraction [%]
1	0.000 - 0.004	47	0.18
2	0.004 - 0.008	47	0.18
3	0.008 - 0.012	47	0.19
4	0.012 - 0.016	48	0.19
5	0.016 - 0.020	47	0.19
6	0.020 - 0.024	47	0.19
7	0.024 - 0.029	47	0.20
8	0.029 - 0.034	48	0.21
9	0.034 - 0.039	47	0.22
10	0.039 - 0.045	47	0.23
11	0.045 - 0.051	47	0.24
12	0.051 - 0.057	48	0.24
13	0.057 - 0.064	47	0.25
14	0.064 - 0.072	48	0.26
15	0.072 - 0.081	47	0.28
16	0.081 - 0.091	47	0.29
17	0.091 - 0.102	47	0.30
18	0.102 - 0.114	47	0.31
19	0.114 - 0.128	47	0.32
20	0.128 - 0.145	47	0.33
21	0.145 - 0.165	47	0.33
22	0.165 - 0.189	47	0.35
23	0.189 - 0.219	47	0.35
24	0.219 - 0.258	47	0.36
25	0.258 - 0.312	48	0.36
26	0.312 - 0.391	48	0.35
27	0.391 - 0.524	48	0.33
28	0.524 - 0.695	49	0.29
29	0.695 - 0.918	53	0.27
30	0.918 - 1.153	58	0.25
31	1.153 - 1.496	59	0.25
32	1.496 - 1.947	56	0.26
33	1.947 - 2.522	66	0.28
34	2.522 - 3.277	62	0.35

QCD fraction in each p_T^Z bin

Bin	Range	Syst. unc. [%]	QCD fraction [%]
1	0.000 - 2.500	47	0.08
2	2.500 - 5.000	48	0.11
3	5.000 - 8.000	48	0.18
4	8.000 - 11.400	47	0.25
5	11.400 - 14.900	47	0.31
6	14.900 - 18.500	47	0.37
7	18.500 - 22.000	47	0.41
8	22.000 - 25.500	47	0.43
9	25.500 - 29.000	47	0.44
10	29.000 - 32.600	47	0.44
11	32.600 - 36.400	47	0.43
12	36.400 - 40.400	48	0.40
13	40.400 - 44.900	47	0.40
14	44.900 - 50.200	48	0.38
15	50.200 - 56.400	49	0.36
16	56.400 - 63.900	48	0.30
17	63.900 - 73.400	51	0.26
18	73.400 - 85.400	56	0.22
19	85.400 - 105.000	68	0.18
20	105.000 - 132.000	80	0.13
21	132.000 - 173.000	91	0.10
22	173.000 - 253.000	71	0.08
23	253.000 - 600.000	48	0.05

QED FSR: Effect of isolated photons with $E_T^\gamma < 200$ MeV

- Photons radiated from an electron outside the cone 0.2 around this electron is considered as isolated.
- Isolated photons with $E_T^\gamma < 200$ MeV are simulated in MC but they are not well calibrated in data.
- MC is used for the unfolding procedure, therefore these photons maybe have an effect on the final result.

$\to$ Cut MC events which have photons radiated from an electron with low E_T^γ (< 10 MeV, < 50 MeV,...) and outside the cone 0.2 around this electron.

$\to$ Compare new C_Z^{norm} with the nominal C_Z^{norm}.

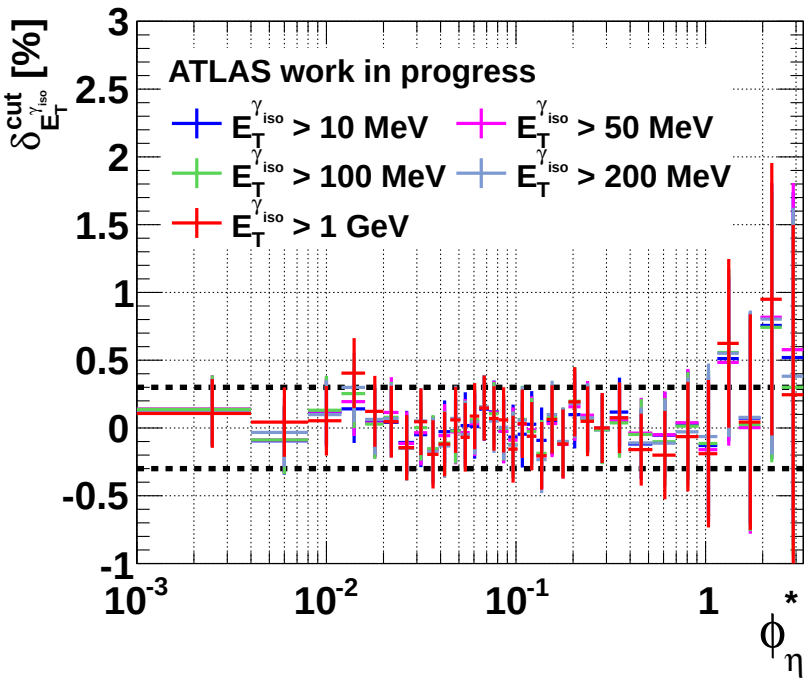

Comparing the p_T^Z results between $Z \to ee$ and $Z \to \mu\mu$ channels